Nuclear Instruments and Methods in Physics Research A 678 (2012) 48–63

Contents lists available at SciVerse ScienceDirect

Nuclear Instruments and Methods in Physics Research A

journal homepage: www.elsevier.com/locate/nima

Effects of errors in velocity tilt on maximum longitudinal compression during neutralized drift compression of intense beam pulses: I. general description

Igor D. Kaganovich [a,*], Scott Massidda [a], Edward A. Startsev [a], Ronald C. Davidson [a], Jean-Luc Vay [b], Alex Friedman [c]

[a] Plasma Physics Laboratory, Princeton University, Princeton, NJ 08543
[b] Lawrence Berkeley National Laboratory, 1 Cyclotron Road, Berkeley, CA 94720
[c] Lawrence Livermore National Laboratory, 7000 East Avenue, Livermore, CA 94550

ARTICLE INFO

Article history:
Received 21 October 2011
Received in revised form
2 March 2012
Accepted 13 March 2012
Available online 21 March 2012

Keywords:
Longitudinal compression
Beam dynamics
Voltage errors

ABSTRACT

Neutralized drift compression offers an effective means for particle beam pulse compression and current amplification. In neutralized drift compression, a linear longitudinal velocity tilt (head-to-tail gradient) is applied to the non-relativistic beam pulse, so that the beam pulse compresses as it drifts in the focusing section. The beam current can increase by more than a factor of 100 in the longitudinal direction. We have performed an analytical study of how errors in the velocity tilt acquired by the beam in the induction bunching module limit the maximum longitudinal compression. It is found that the compression ratio is determined by the relative errors in the velocity tilt. That is, one-percent errors may limit the compression to a factor of one hundred. However, a part of the beam pulse where the errors are small may compress to much higher values, which are determined by the initial thermal spread of the beam pulse. It is also shown that sharp jumps in the compressed current density profile can be produced due to overlaying of different parts of the pulse near the focal plane. Examples of slowly varying and rapidly varying errors compared to the beam pulse duration are studied. For beam velocity errors given by a cubic function, the compression ratio can be described analytically. In this limit, a significant portion of the beam pulse is located in the broad wings of the pulse and is poorly compressed. The central part of the compressed pulse is determined by the thermal spread. The scaling law for maximum compression ratio is derived. In addition to a smooth variation in the velocity tilt, fast-changing errors during the pulse may appear in the induction bunching module if the voltage pulse is formed by several pulsed elements. Different parts of the pulse compress nearly simultaneously at the target and the compressed profile may have many peaks. The maximum compression is a function of both thermal spread and the velocity errors. The effects of the finite gap width of the bunching module on compression are analyzed analytically.

Published by Elsevier B.V.

1. Introduction

Longitudinal compression is a standard technique used to increase the beam intensity in various accelerators [1]. Longitudinal compression during neutralized drift is achieved by accelerating the tail of the beam pulse relative to the head. This is accomplished experimentally by passing the beam pulse through a time-dependent bunching module and then through a plasma region where the beam space charge is neutralized. Previous longitudinal drift compression analysis has studied the effects of intrinsic beam momentum spread, plasma, and solenoidal final focus conditions on compression [1,2]. Much focus has also gone towards space-charge neutralization [1,3,4], where it was shown that plasma can neutralize the space charge and current of the beam to a very high degree, sufficient to provide neutralized ballistic focusing. The kinematics of neutralized drift compression is well-developed [5,6]. In the case of an ideal (perfect) velocity tilt, all beam ions arrive at the same location at the target plane and the beam compression is determined by intrinsic velocity spread. In practical devices, the bunching module operates with some errors in voltage, which results in errors in the velocity tilt. Due to errors in the velocity tilt, the beam ions arrive at the target plane at different times, which limits the compression and determines the final shape of the pulse at the target. Typically, the velocity errors are much bigger than the intrinsic thermal spread. Therefore, the effects of

* Corresponding author. Tel.: +1 609 243 3277; fax: +1 609 243 2418.
E-mail address: ikaganov@pppl.gov (I.D. Kaganovich).

0168-9002/$ - see front matter Published by Elsevier B.V.
http://dx.doi.org/10.1016/j.nima.2012.03.007

errors in the velocity tilt on the longitudinal compression dominate the thermal effects. The effects of errors are mostly responsible for the final pulse compression and are the main subject of this paper. Correspondingly, we analyze a few possible scenarios for how the errors in the velocity tilt acquired by the beam in the bunching module can limit the beam compression for future and current accelerators. This analysis should give designers of the bunching module the necessary conditions for the accuracy of the voltage form on the bunching module. An accompanying paper [7] applies the obtained results to experimental data from the Neutralized Drift Compression eXperiment-I (NDCX-I) [8–10].

We have performed an analytical study of how errors in the velocity tilt acquired by the beam in the induction bunching module can limit the maximum longitudinal compression. Due to errors in the velocity, δv_b, the beam pulse width at the target plane, l_f, is of order $\delta v_b t_f$, where t_f is the time to reach the target plane. Correspondingly, the width of the beam pulse is decreased from the initial pulse width, $v_{b0}t_p = l_p$, to $\delta v_b t_f$. Here, v_{b0} and t_p are the initial beam velocity and pulse duration, respectively. This gives a compression ratio of the order

$$C \sim \frac{l_p}{l_f} = \frac{v_{b0} t_p}{\delta v_b t_f} \tag{1}$$

The time to reach the target plane is related to the applied velocity tilt Δv_b by

$$\Delta v_b t_f = l_p \tag{2}$$

so that the beam ions from the tail overtake the beam ions at the head at the target plane after drifting in the compression section. Typically, the pulse duration is much shorter than the focusing time, $t_p \ll t_f$, and the velocity modulation is small compared with the initial beam velocity, $|\Delta v_b| < v_{b0}$, with the fractional velocity tilt, $Max(\Delta v_b)/v_{b0}$, of order 5–30%. Substituting Eq. (2) into Eq. (1) gives

$$C \sim \frac{\Delta v_b}{\delta v_b} = \frac{\Delta U}{\delta U} \tag{3}$$

Therefore, the compression ratio is limited by the relative errors in the applied velocity tilt in the induction bunching module, compared with the ideal velocity tilt [11], and are related to the voltage errors in the induction bunching module. Here, $\Delta U = M v_b \Delta v_b$ is the amplitude of the voltage, and $\delta U = M v_b \delta v_b$ is a typical value of the voltage error. Similarly, the minimum compressed pulse duration is $\delta t_p \sim \delta v_b t_f / v_b = \delta v_b t_p / \Delta v_b$, and is also determined by the voltage errors according to

$$\delta t_p \sim t_p \frac{\delta U}{\Delta U} \tag{4}$$

Typical values of the relative error in the voltage of the induction bunching module are about 1–2%. Eq. (3) then gives a compression, C, in the range $C \sim 50$–100. This estimate agrees well with the reported values of longitudinal compression obtained in experiments [8–10,12]. If there were no errors in the velocity tilt, then the effects associated with a small thermal velocity v_T ($v_T = \sqrt{2T_{bz}/M}$ and $T_{bz} \sim 0.2eV$) would limit the compression in Eq. (3) to a value of order

$$C_T \sim \frac{\Delta v_b}{v_T} \tag{5}$$

For example, for the 300 keV beam in NDCX-I, $v_{b0}/v_T \sim 1000$ and $C_T \sim 300$ for a velocity tilt $\Delta v_b / v_{b0} \sim 1/3$ [10]. However, this would require a very precise design of the induction bunching module with an error of order 0.1%; and, similarly, the control of the beam velocity in the ion source should be realized with a precision within 0.1%.

If the value of the error $\delta v_b/\Delta v_b$ is much smaller for a part of the beam pulse, then this part of the beam pulse may compresses to high values, whereas the rest of the pulse does not compress well. For important practical cases, the analysis of compression is more complicated because both the thermal spread and errors in the velocity tilt should be considered simultaneously. This requires a kinetic treatment of the longitudinal compression. Analytical formulas for the beam profile dynamics have been derived and can be used for practical calculations of the longitudinal compression. We shall consider three cases: the first two cases deal with a smooth variation of errors over the beam pulse; the first one with relatively large errors, $\delta v_b/\Delta v_b \sim 10\%$, and the second case with smaller errors, $\delta v_b/\Delta v_b \sim 1\%$. For the third case, we consider errors of similar size to the second case, $\delta v_b/\Delta v_b \sim 1\%$, but rapidly changing during the pulse. This corresponds to a technical realization of the induction bunching module consisting of many independent elements, each introducing an error.

For the case of smooth errors, where only a small portion of the pulse compresses, it is found that the resulting beam profile at the target plane has a very wide foot described by a power law, and the central part is determined by the shape of the distribution function in thermal velocity spread. For the case of rapidly changing errors during the pulse, the resulting maximum compression depends weakly on the thermal spread, because the velocity tilt errors dominate the thermal spread effects at all times.

This paper is organized as follows: Section 2 provides the basic equations in both Lagrangian and Eulerian descriptions, Section 3 considers general properties of the effects of voltage errors and thermal spread on the longitudinal compression, Section 4 analyzes the effects of the finite gap of the induction bunching module, and Section 5 summarizes the conclusions. Appendixes A and B provide additional details on general properties of current density profiles of compressed pulse for slowly-varying voltage errors compared to voltage pulse on the bunching module.

2. Basic equations

2.1. Lagrangian description in parametric form neglecting thermal effects

First, we consider beam compression neglecting the thermal spread. After the beam pulse passes through a time-dependent bunching module, the beam acquires the velocity tilt, $\Delta v_b(\tau)$, where τ is the time of beam interaction with the induction bunching module. The beam then passes through a plasma region where the beam space charge is neutralized and space charge effects can be neglected. The time τ can be viewed as a marker of the beam pulse slice, or as a Lagrangian coordinate. The resulting change in the beam velocity, $\Delta v_b(\tau)$, during the pulse interval, $0 \le \tau \le t_p$, should be chosen so that all of the beam ions arrive simultaneously at the same focal plane at a distance, l_f, from the location of the induction bunching module. Here, we consider a continuous long beam, a part of the beam is compressed by passing through a bunching module. For example, for NDCX-I experiment about 500 ns of the 10 μs beam is compressed. The rest of the beam $\tau < 0$ and $\tau > t_p$ is not compressed at the target plane. The ion beam dynamics can be described analytically by following the ion beam trajectory, $z_b(t,\tau)$ as a function of time, t. The following equation expresses the beam dynamics in a parametric form as a function of the time variables, t and τ. The ion beam trajectory after passing an induction bunching module for $t > \tau$ is given by

$$z_b(t,\tau) = v_b(\tau)(t-\tau), \tag{6}$$

where $v_b(\tau) = v_{b0} + \Delta v_b(\tau)$ is the beam velocity after the bunching module, and $v_{b0} \equiv v_b(0)$ is the beam velocity after interaction with

the induction bunching module at the beginning of the pulse. For simplicity, both time variables t and τ are counted from this moment. Note, that the initial beam velocity before interaction with the induction bunching module, v_b^{in}, can be different from v_{b0}, because the beam head and sometimes the entire pulse is often decelerated relative to other uncompressed parts of the beam. The position of a beam ion before interacting with the induction bunching module at time τ, i.e., for $t<\tau$ is

$$z_0(\tau)=v_b^{in}(t-\tau) \tag{7}$$

The condition for longitudinal compression is that all parts of the compressed beam pulse arrive simultaneously at the same location, i.e.,

$$z_b(t_f,\tau)=l_f, \tag{8}$$

for all τ (see Fig. 1 for a schematic of the beam trajectories during compression – the so-called 'Applegate' diagram for velocity modulation [13,14]). Here, $t_f=l_f/v_{b0}$ is the time-of-flight of the beam pulse from the bunching module to the final focus plane. From Eqs. (6) and (8) it follows that the ideal velocity tilt, $\Delta v_b^i(\tau)$ should satisfy [15,6]

$$\Delta v_b^i(\tau)=v_{b0}\tau/(t_f-\tau), \quad or; \quad v_b^i(\tau)=v_{b0}t_f/(t_f-\tau) \tag{9}$$

The ion line density can be determined from the compression of the beam pulse, dz_b/dz_0, where dz_0 is the initial distances between two slices, and dz_b is the current distance. Here, we consider only longitudinal dynamics and do not consider possible simultaneous radial compression. In neutralized ballistic focusing, the radial and longitudinal compressions are dynamically decoupled; therefore, once the longitudinal dynamics is known, the transverse focusing (which is affected by chromatic aberrations) can be studied independently. Thus, in the following, by "ion beam density" we are referring to "ion beam line density". The initial position of a beam ion interacting with the induction bunching module is given by Eq. (7) and the current position is given by Eq. (6). Therefore, the ion line density is given by

$$n_b(\tau,t)=n_b^{in}\left|\frac{dz_0}{dz_b}\right|=\frac{n_b^{in}v_b^{in}}{|\partial z_b/\partial\tau|} \tag{10}$$

Here, n_b^{in} is the beam line density before the bunching module, which we assumed constant for a long coasting beam produced by the ion source. Substituting $z_b(t,\tau)$ from Eq. (6) into Eq. (10) gives

$$\frac{\partial z_b}{\partial\tau}=(t-\tau)dv_b(\tau)/d\tau-v_b(\tau), \tag{11}$$

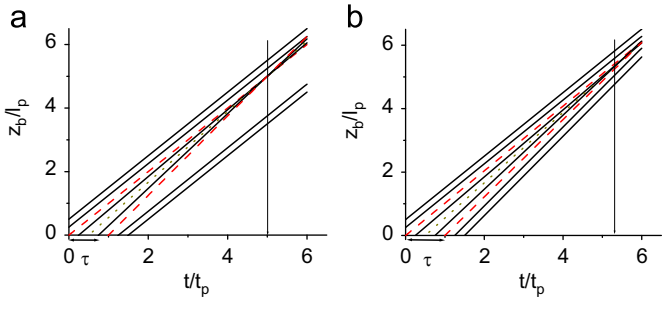

Fig. 1. Schematic of the beam trajectories during compression, -'Applegate' diagram for velocity modulation. The arrows indicate the time τ when the beam passes through the tilt core, which changes the beam velocity. (a) The ideal velocity tilt given by Eq. (9) when the entire beam pulse is compressed at the target plane; (b) the velocity tilt with errors shown in Fig. 4. Dashed (red) lines show boundaries of the beam pulse. Dotted (dark yellow) line shows the middle of the pulse. All units are normalized to the pulse duration, t_p, and the pulse length, l_p. (For interpretation of the references to color in this figure legend, the reader is referred to the web version of this article.)

$$n_b(\tau,t)=\frac{n_b^{in}v_b^{in}}{|v_b(\tau)-(t-\tau)dv_b(\tau)/d\tau|} \tag{12}$$

Eq. (12) has been generalized in Refs. [16–18] taking into account thermal effects and space-charge effects. From Eq. (12) it follows that the compression ratio in the current density is given by

$$C_j(\tau,t)=\frac{n_b(\tau,t)v_b(\tau)}{n_b^{in}v_b^{in}}=\frac{1}{|1-(t-\tau)d\ln v_b(\tau)/d\tau|} \tag{13}$$

Substituting $z_b(t,\tau)$ from Eq. (6) into Eq. (13) gives the current compression ratio as a function of the variables z and τ traditionally used in klystron theory [13,14]. Note that in contrast to klystron theory, where the voltage is assumed to be a harmonic function, voltage in the inductive bunching module is very different from a harmonic function. Therefore, some of the features of compressed pulse are very different from the klystron case. The compression ratio can be expressed as a function of (τ,z) according to

$$C_j(\tau,z)=\frac{1}{|1-z(dv_b(\tau)/v_b(\tau)^2d\tau)|} \tag{14}$$

Note that due to current conservation $C_j(\tau,t)=1$ at $t=\tau$, i.e., right after passing the induction bunching module. In the following, we shall use both the compression ratio for the beam line density and the current density; they differ by the ratio of the instantaneous and initial beam velocities and can be easily converted from one to the other. A convenient way to characterize the compression of the pulse is to introduce the time, $t_s(\tau)$, when different parts of the ion beam pulse compress or when neighboring slices of the beam arrive at the same position. In Lagrangian coordinates, this corresponds to a singularity of the beam line density profile given by Eq. (12), i.e., at time

$$t_s(\tau)=\frac{v_b(\tau)}{dv_b(\tau)/d\tau}+\tau \tag{15}$$

Substituting Eq. (15) into Eq. (12) gives the compression ratio, n_b/n_b^{in}, as a function of τ

$$C\equiv\frac{n_b(\tau,t)}{n_b^{in}}=\frac{1}{|t-t_s(\tau)|}\frac{v_b^{in}}{dv_b(\tau)/d\tau} \tag{16}$$

Because $v_{b0}/dv_b(\tau)/d\tau\approx t_f$, the compression ratio at time $t=t_f$ $C\approx t_f/|t_f-t_s(\tau)|$. In the case of ideal compression, all parts of the beam pulse compress at the same time, t_f. However due to errors in the applied velocity tilt, different parts of the beam pulse compress at different times $t_s(\tau)\neq t_f$, and correspondingly the compression ratio is inversely proportional to the relative error in the time of compression of different parts of the beam pulse

$$C\approx\frac{t_f}{\delta t_s(\tau)} \tag{17}$$

Here, $\delta t_s(\tau)=t_s(\tau)-t_f$.

2.2. Eulerian description neglecting thermal effects

It is instructive to compare the Lagrangian solution given by Eq. (12) with the solution in Eulerian coordinates; see, for example, Refs. [16,17]. After the beam pulse passes through the bunching module completely at time $t=t_p$, the beam velocity has a profile as a function of z, and corresponding gradient $\partial v_b/\partial z(z,t_p)$ and line density profile $n_b(z,t_p)$. The solution to the fluid equations for free convection

$$\frac{\partial n}{\partial t}+\frac{\partial v_b n}{\partial z}=0, \tag{18}$$

can be expressed as [17]

$$n(z,t)=\frac{n_b(z,t_p)}{1+(\partial v_b(z,t_p)/\partial z)(t-t_p)} \tag{19}$$

Here, functions $n_b(z,t_p)$ and $\partial v_b/\partial z(z,t_p)$ can be determined from functions $n_b(\tau,t_p)$ given by Eq. (12) and $z=z_b(t,\tau)$ determined from Eq. (6) for a given τ; the gradient of the beam velocity established by the bunching module is given by

$$\frac{\partial v_b(z,t)}{\partial z}=\frac{\partial v_b/\partial\tau}{\partial z_b/\partial\tau}=-\frac{1}{(1/d\ln v_b(\tau)/d\tau)-(t-\tau)}, \tag{20}$$

where $\partial z_b/\partial\tau$ was used from Eq. (11). Substitution of the ideal profile given by Eq. (2) into Eq. (20) gives

$$\frac{\partial v_b(z,t_p)}{\partial z}=-\frac{1}{t_f-t_p}, \tag{21}$$

i.e., the established velocity gradient after the beam pulse passes through the bunching module is constant and the velocity profile is linear.

The solution is also convenient to consider in the phase-space (z,v), where each point moves with velocity v along the z-axis, so that a straight line in phase space with a constant slope remains a straight line in phase space and compresses into a vertical line [17,20] (see Fig. 2).

Another informative way to characterize the errors is to calculate the errors in the applied velocity gradient after the beam has passed through the bunching module. The first time a part of the beam compresses corresponds to the maximum value of the velocity gradient $-\partial v_b/\partial z|_{\max}$ at the time when Eq. (19) gives a singularity, i.e.,

$$t_{\min}=t_p-\frac{1}{\partial v_b/\partial z|_{\max}} \tag{22}$$

From Eq. (19) it is evident that the compression ratio at time $t_{\min}$ is given by

$$C(z,t_{\min})\equiv\frac{n_b(z,t)}{n_b^{in}}=\frac{n_b(z,t_p)/n_b^{in}}{[(\partial v_b/\partial z)-(\partial v_b/\partial z)|_{\max}](t_{\min}-t_p)} \tag{23}$$

That is, the compression ratio is inversely proportional to the error in the applied velocity gradient and time to compression. Because $t_{\min}-t_p=1/[\partial v_b/\partial z|_{\max}]$ and for small amplitude velocity tilt $\Delta v_b(\tau)\ll v_b^{in}$, $n_b(z,t_p)\approx n_b^{in}$, the compression ratio is inversely proportional to the relative error in the velocity gradient, i.e.,

$$\frac{C(z,t)\approx\partial v_b/\partial z|_{\max}}{[\partial v_b/\partial z-\partial v_b/\partial z|_{\max}]} \tag{24}$$

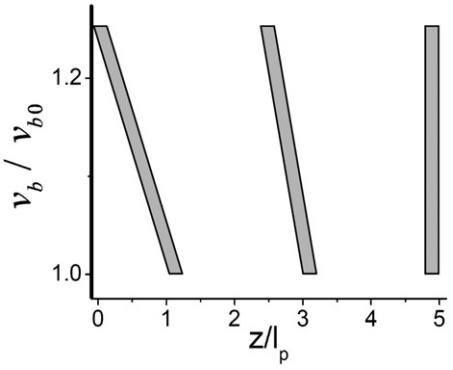

Fig. 2. The phase-space during ideal compression with a linear velocity gradient. Shown are the normalized beam velocity as a function of the normalized position for three times: $t/t_p=1$; 3; 4.9. The initial profile at $t/t_p=1$ is $v_b/v_{b0}=1+0.25(1-z/l_p)$, and $l_p=v_{b0}t_p$ is the length of the pulse. The pattern schematically shows the spread in phase space due to thermal effects.

The relation between the velocity gradient and the velocity tilt as a function of time is given by Eq. (20). The time function, $t_s(\tau)$, when different parts of the ion beam pulse compress can be used instead of the velocity gradients. Both functions are related according to Eq. (20) and Eq. (15) by

$$\frac{\partial v_b(z,t)}{\partial z}=-\frac{1}{t_s(\tau)-t};\quad z=z_b(t,\tau) \tag{25}$$

For a small velocity tilt and error in the velocity modulation with $|\delta v_b|\ll|\Delta v_b|\ll v_b^{in}$, expanding Eq. (15) in $\delta v_b/\Delta v_b^i$, where Δv_b^i is given by Eq. (9), yields

$$t_s(\tau)\simeq t_f\left[1+\frac{\delta v_b}{v_{b0}}-t_f\frac{d\delta v_b/d\tau}{v_{b0}}\right] \tag{26}$$

Note that because the velocity error changes with time on a time scale short compared to the focusing time, $t_p\ll t_f$, the third term in Eq. (26) typically dominates the second term. Making use of the estimates, $d\delta v_b/d\tau\sim\delta v_b/t_p$ and $t_f/t_p\sim v_b/\Delta v_b$, gives for the influence of errors on the compression time

$$\frac{\delta t_s(\tau)}{t_f}\sim\frac{t_f d\delta v_b/d\tau}{v_{b0}}\sim\frac{\delta v_b}{\Delta v_b} \tag{27}$$

Substituting Eq. (27) into Eq. (17) gives

$$C\sim\frac{t_f}{\delta t_s}\sim\frac{\Delta v_b}{\delta v_b} \tag{28}$$

That is, the compression ratio is inversely proportional to the relative errors in the velocity tilt.

2.3. Lagrangian description in parametric form taking thermal effects into account

2.3.1. Discussion of effects of thermal spread on maximum compression

A singularity in the expression of the compression ratio in Eqs. (12) or (19) is limited by thermal effects. Therefore, these equations have been generalized, taking into account small thermal effects. For the ideal velocity profile given by Eq. (9), the beam line density tends to infinity at $t=t_f$ independently of τ for any slice of the beam pulse, corresponding to perfect compression. The singularity is limited due to effects of the finite temperature or energy spread of the beam [18,9]. Due to the small energy spread, ions arrive at different locations at time t_f even for an ideal velocity tilt. Correspondingly, the spread of positions around the compression location appears over distances $v_T t_f$, where v_T is the thermal component of the beam velocity associated with the beam energy spread. The thermal spread can be described by the velocity distribution function, $f(v)$, in the ion source before acceleration through the bunching module, e.g., by a Maxwellian velocity distribution function $f(v)=n_0\exp(-v^2/v_T^2)/v_T\sqrt{\pi}$. For a beam pulse with a Maxwellian velocity distribution function the profile is given by

$$n_b(z,t_f)=\frac{n_b^{in}t_p v_b^{in}}{\sqrt{\pi}v_T t_f}\exp\left(-\frac{(z-l_f)^2}{t_f^2v_T^2}\right) \tag{29}$$

The maximum compression ratio $C\equiv n_b/n_b^{in}$ given by Eq. (29) becomes

$$C_{\max}=\frac{t_p v_b^{in}}{\sqrt{\pi}v_T t_f} \tag{30}$$

which is the ratio of the initial beam pulse width to the width of the compressed pulse due to thermal spread. For example, for NDCX-I parameters, the ion beam energy is 300 keV, and $T_{bz}\simeq 0.3eV$, $v_T/v_{b0}\approx 10^{-3}$; and for a velocity tilt, $\Delta v_b/v_{b0}=t_p/t_f=0.15$ [10], Eq. (30) gives $C_{\max}=84$. For NDCX-II parameters with initial 12 active induction cells, the ion beam energy is

3 MeV, and $T_{bz} \simeq 0.3eV$, $v_T/v_{b0} \approx 3\times10^{-4}$; and for a velocity tilt $\Delta v_b/v_{b0}=t_p/t_f=0.25$ [19], Eq. (30) gives $C_{\max}=470$. The above estimates for the maximum achievable compression strongly rely on assumptions about the longitudinal temperature.

2.3.2. Discussion of longitudinal temperature

The beam longitudinal temperature and the corresponding energy spread develop due to several effects. The initial spread in the beam energy, ΔE_i, is determined by the temperature of the ion source, T_i; i.e., $\Delta E_i=T_i=500$–1200 K$=0.05$–0.12 eV. After acceleration in the diode of the ion source, the beam energy spread, ΔE_{bz}, remains unchanged due to conservation of energy, $\Delta E_{bz}=\Delta E_i=T_i$, whereas the beam temperature strongly decreases due to acceleration cooling, $T_{bz}=T_i^2/2E_b$. For NDCX-1 expected temperature due to acceleration cooling would be $T_{bz}=T_i^2/2E_b\sim10^{-8}eV$. Note that the temperature in the perpendicular direction remains the same, $T_{b\perp}=T_i$ [20].

Ref. [6] suggested several possible mechanisms for increasing the energy spread, including two-dimensional effects in the diode, and collective effects due to the beam space charge. A detailed numerical study of both effects was performed; the study made it clear that neither mechanism leads to significant energy spread [21]. The energy spread and the beam kinetic energy are shown in Fig. 3. It is evident from Fig. 3 that there is no energy spread increase due to two-dimensional effects in the diode region as opposed to the conjecture in Ref. [6]. The two degrees of freedom of the beam kinetic energy along and across the z-axis are not coupled. The space charge of the beam results in the beam ions in the center of the pipe slowing down, as shown in Fig. 3. However, as the beam exits to the plasma or the extraction metal plate under experimental conditions, this difference in kinetic energy is removed, as evident in Fig. 3 at $z=3$ m, because the plasma or the extraction metal plate are equipotentials. The simulations thus predict a very small energy spread of several eV in the beam ions.

However, the measured energy spread in NDCX-1 device is about $\Delta E_{bz}\le100$ eV [12]. The corresponding beam temperature for $\Delta E_{bz}=100$ eV, $T_{bz}=0.05$ eV, does not correspond to the acceleration cooling [22]. The Boersch effect may be responsible for the temperature equipartitioning, $T_{bz}=T_{b\perp}$ [20,23], caused by the beam-beam particle Coulomb collisions, or the equipartitioning can be caused by collective instabilities [24]. Another possible effect is the voltage drift during acceleration in the diode, which results in beam energy variation during the pulse. Currently, the experimental studies of the longitudinal temperature and energy spread have not been adequate to resolve this question.

Therefore, in the following we shall assume that $T_{bz}=T_i$, and that the value is determined by the ion source temperature.

Note that a thermal equilibrium distribution in the beam energy,

$$f_M(v)=\frac{1}{\sqrt{2\pi T_z/M}}\exp\left(-\frac{M(v-v_b)^2}{2T_z}\right)$$

corresponds to a Gaussian distribution in the energy spread $\Delta E_b\approx M(v-v_b)v_b$ with

$$f_M(\Delta E)=\frac{1}{\sqrt{2\pi T_z/M}}\exp\left(-\frac{(\Delta E)^2}{4E_bT_z}\right)$$

Correspondingly, the standard deviation of the energy spread is $2\sqrt{E_bT_z}$; the average dispersion of the energy spread is $\sqrt{\left\langle(\Delta E)^2\right\rangle}=\sqrt{2E_bT_z}$; and the full width half maximum (FWHM) of the energy spread is $2\sqrt{E_bT_z\ln(2)}$. For example, for $T_{bz}\simeq0.1eV$ and $E_b=300$ keV, the energy spread dispersion is 245 eV and the standard deviation is 347 eV.

2.3.3. Discussion of voltage errors

Another effect that can prevent ions from arriving at the same location at the same time is associated with the errors in the applied velocity tilt due to the difference (error) in the voltage of the bunching module with the required voltage pulse by the ideal velocity tilt. Typically, errors in the applied velocity tilt are significantly larger than the beam energy spread before the bunching module. Typical values of the relative error in the induction bunching module, $\delta v_b/\Delta v_b$, are about 1–5% and are typically higher than the thermal effects $v_T/\Delta v_b\sim0.3\%$. For example, in NDCX-1 experiments, the energy spread is 170 eV, whereas errors in the applied voltage of the bunching module can reach 2 kV [22]. Therefore, the effects of errors in the velocity tilt on the longitudinal compression dominate the thermal effects and are the main subject of this section. In general, both effects have to be taken into account in a full kinetic treatment.

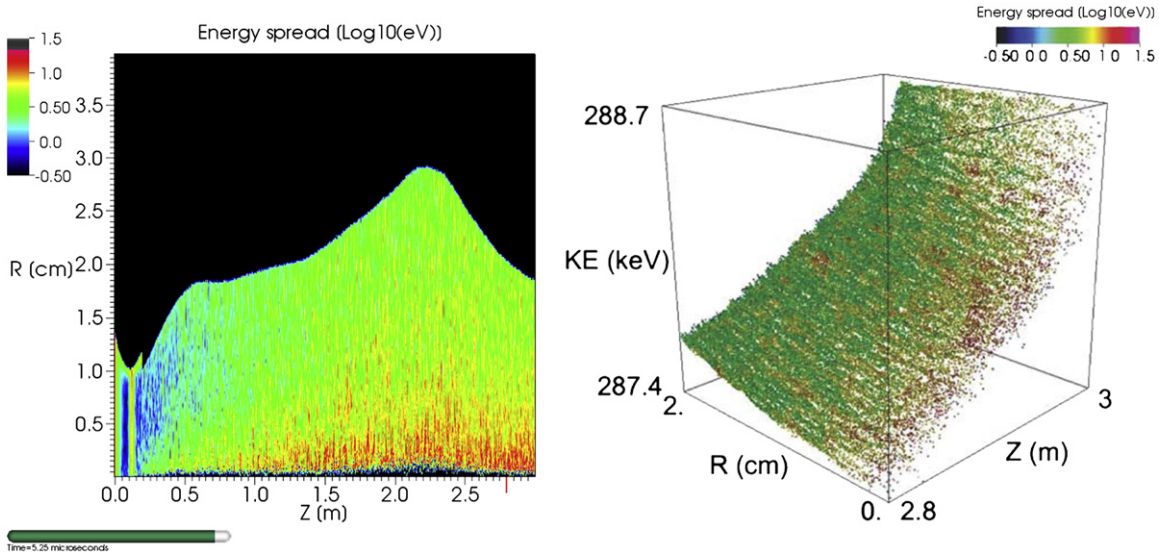

Fig. 3. The colorplot of energy spread (left) superimposed on the beam kinetic energy (right) in the NDCX-I device simulated by the WARP particle-in-cell code in Ref. [21].

2.3.4. Calculating compression in the kinetic approach

A calculation of the beam density in a kinetic approach can be performed analytically by considering the number of beam particles in phase space at a given location within an interval dz. Taking a small thermal velocity, v_T, into account, the particle trajectory becomes $z=z_b(t,\tau)+vt$. The distribution function is constant along the ballistic trajectories. The line density of the beam is given by the number of beam particles in phase space at a given location [9], for continues initial beam which gives

$$n_b(z,t)=\int_{-\infty}^{t} v_b^{in} d\tau \int_{-\infty}^{\infty} dv f(v)\delta(z-z_b(t,\tau)-vt) \tag{31}$$

where v is the particle's velocity increment associated with the thermal spread. Integrating once over velocity gives

$$n_b(z,t)=\frac{v_b^{in}}{t}\int_{-\infty}^{t} d\tau f\left(\frac{z-z_b(t,\tau)}{t}\right) \tag{32}$$

If the thermal spread is sufficiently small, the distribution function can be changed to a delta-function $f(v)\to\delta(v)$, and Eq. (32) becomes the same as Eq. (10). In the limit of ideal compression when the entire beam pulse compresses, the maximum compression is given by the ratio of the initial beam pulse length to the length of the pulse associated with the thermal spread (see Fig. 2). The thermal spread length is determined approximately by the distance a beam particle moves at the thermal velocity in the positive and negative directions, $\pm v_T t_f$. In the case of non-ideal compression with large errors in the velocity tilt, the beam density is determined by the portion of the phase space that compresses within a distance $\pm v_T t_f$ from the location of the maximum compression; and the maximum compression is given by the ratio of the initial length of the fraction of the beam pulse that compresses within the thermal spread length (see Fig. 5(b)). The ion beam line density given by Eq. (32) can be rewritten as

$$n_b(\tau,t)=n_b^{in}\left|\frac{v_b^{in}\Delta\tau}{2v_T t_f}\right|, \tag{33}$$

where we introduced the fraction of the beam pulse $\Delta\tau(t,\tau)/t_p$ that compresses within the thermal spread width, i.e., the range of values $\delta\tau$ such that, $z_b(t_f,\tau+\delta\tau)\in[z_b(t_f,\tau)-v_T t_f, z_b(t_f,\tau)+v_T t_f]$. Here,

$$\Delta\tau(t,\tau)=\frac{2v_T}{n_b^i}\int d\tau f\left(\frac{z-z_b(t,\tau)}{t}\right)$$

If the function $z_b(t,\tau)$ has non-zero derivative $\partial z_b(t,\tau)/\partial\tau$ then the very small thermal spread is not important and the distribution function can be substituted by a delta-function, $f(v)\to n_b^i\delta(v)$ and

$$\Delta\tau(t,\tau)=\frac{2v_T t}{\partial z_b(t,\tau)/\partial\tau} \tag{34}$$

Therefore, the generalized expression for the beam line density given by Eq. (32) or Eq. (33) takes into account the thermal spread effects and tends to the previous expression if the thermal effects are not important, and describes limitations at the singular locations due to thermal effects when and where the beam pulse compresses.

In the following sections, specific examples showing the influence of errors on compression are described in more detail. We consider first two cases: one with relatively large errors $\delta v_b/\Delta v_b\sim 10\%$, and the other with small errors $\delta v_b/\Delta v_b\sim 1\%$. We show that even for large errors, the local value of compression can be large, whereas the average value of compression over the entire pulse is small. Only in the case when the errors are small can the average value of compression over the entire pulse be large.

3. General properties of the Effects of voltage Errors and thermal spread on the longitudinal compression

3.1. Case 1: relatively large errors ($\delta v_b/\Delta v_b\sim 10\%$) in velocity modulation

The ideal beam velocity modulation function given by Eq. (9) has a discontinuity in the derivative at the beginning of the pulse $\tau=0$, and a discontinuity in the function at the end of the pulse $\tau=\tau_p$, as shown in Fig. 4. An example of a velocity modulation described by a smooth function at the beginning and the end of the pulse is shown in Fig. 4. The absolute value of the error in the velocity $\delta v_b/v_b$ is below one percent for most of the pulse, $0.1<\tau/t_p<0.8$. Detailed analysis of the compression can be found in Appendix A. Here we summarize key results.

The phase-plot evolution is shown in Fig. 5. From Fig. 5 it is evident that a central part of the beam pulse compresses first at time $t/t_p=5.32$ and the head and the tail of pulses compress later in time. The compression ratio is shown in Fig. 6 for $v_T/v_{b0}=2\times10^{-4}$, and comparison with the case where $v_T/v_{b0}=10^{-3}$ is shown in Fig. A5 of Appendix A. For the case of relatively large errors, $\delta v_b/\Delta v_b\sim 10\%$ in the velocity tilt, the central part of beam pulse where the velocity tilt errors are small compresses well, whereas the rest of the pulse does not. The compression ratio for most of the remaining pulse is low ~ 10 (see Figs. 6 and A5 of Appendix A). The maximum compression $C\approx v_{b0}\Delta\tau/2v_T t$ is given by the ratio of the width of the part of the beam pulse, $v_{b0}\Delta\tau$, which compresses to within the thermal spread length, $2v_T t$. Here, $\Delta\tau(t,\tau)/t_p$ is the fraction of the beam pulse that compresses within the thermal spread length, $2v_T t$. The compressed beam profile in the center is determined by thermal effects and reflects the particle distribution function; the broader wings of the profile are determined by the errors in the applied velocity tilt. Because of the velocity tilt errors, the tail and the head of the pulse compress at a later time than the central part of the pulse. At these times, the compressed beam profile has a double peak structure (both as a function of z for a given time or a function of time at a given z). Because at this time the tail of the pulse overtakes the head, the first peak in the double-peak structure corresponds to the tail, and the second peak to the head (see Fig. 6 for $t_{ob}/t_p=5.5;5.9$ and $z_{ob}=5.54;5.98l_p$). The double peak structure is a well-known phenomenon in the klystron theory [13,14] and was also observed in experiments with an inductive bunching module [25] and in previous simulations of longitudinal compression [9]. Note that this double-peak structure has rapid rise and low "foot" compared with the case when beam first compresses (compare

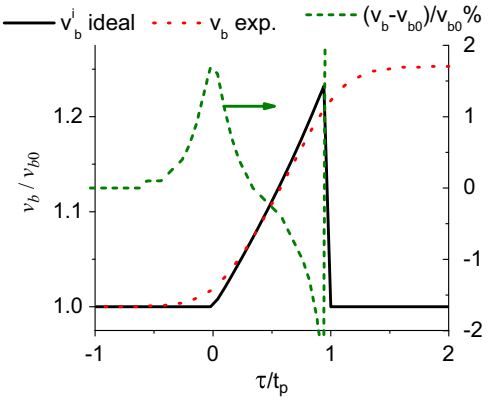

Fig. 4. The normalized beam velocity v_b/v_{b0} as a function of normalized time, τ/t_p in the tilt core. The solid curve shows the ideal velocity variation given by Eq. (9). The dotted (red) curve shows a model of the velocity tilt in experiments, and the dashed curve (green) shows the value of the error in percent. (For interpretation of the references to color in this figure legend, the reader is referred to the web version of this article.)

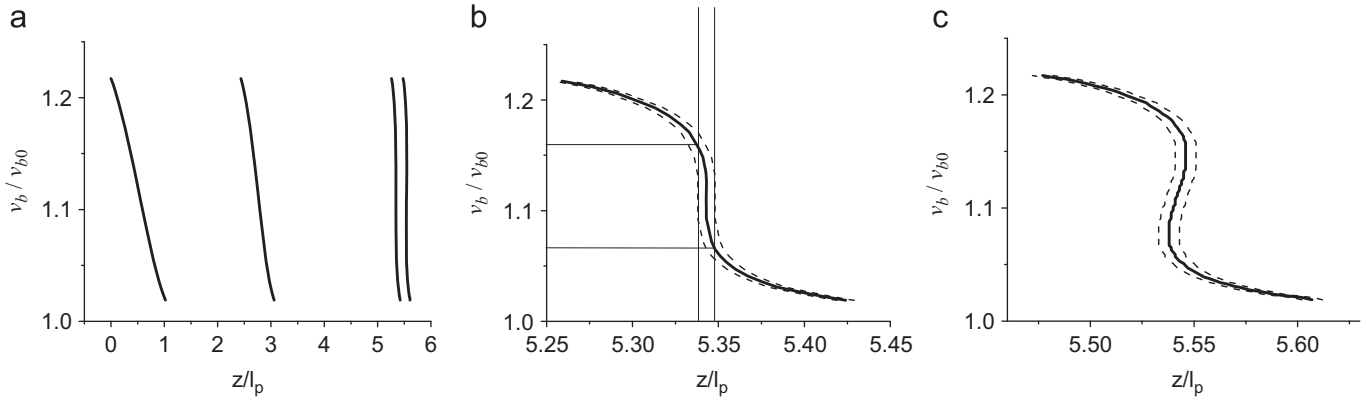

Fig. 5. Phase-space during compression. Shown are plots of the normalized beam velocity as a function of the normalized position for (a) the four times $t/t_p=1$; 3; 5.32;5.5; (b) zoom-in at $t/t_p=5.32$; and (c) zoom-in at $t/t_p=5.5$ for the velocity tilt shown in Fig. 4. The dashed lines in (b) show the spread of the phase space distribution due to thermal effects; the horizontal lines show the velocity width of the phase-space at the location of maximum compression. Note that the heads and tails of these pulses are not expected to compress and are not present in the ideal velocity tilt represented in Fig. 2. Note that a small horizontal shift on $v_T t_f$ is hardly seen on horizontal part of the phase space plot for head or tail of the beam.

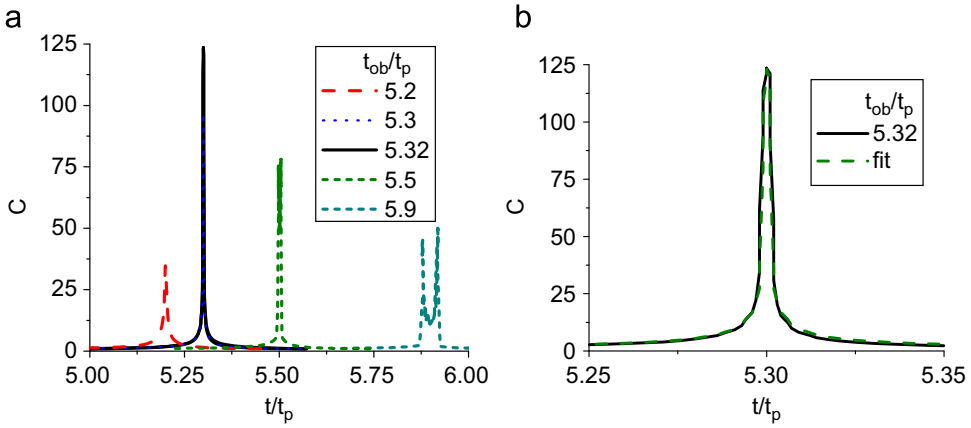

Fig. 6. (a) Plot of the compression ratio as a function of time t/t_p at five different locations $z_{ob}=z_b(t_{ob},0.5t_p)$ with $t_{ob}/t_p=5.2;5.3;5.32;5.5;5.9$ ($z_{ob}=5.21;5.31;5.34;5.54;5.98l_p$) chosen so that the center of the pulse arrives at the target plane at a given time t_{ob}. The maximum compression is limited by thermal effects with $v_T/v_{b0}=2\times10^{-4}$. (b) shows a zoom-in of the compression ratio as a function of time at the optimum compression location at $z_{ob}=z_b(t_{\min},0.5t_p)=5.34l_p$ and $t_{ob}=t_{\min}=5.32t_p$ (black solid curve), and the approximation given by Eq. (63) (dashed green curve), for times $|t-t_{\min}|>v_T t_f/v_b$, and $C_f(t)$ is determined by the thermal spread and is described by a Gaussian function in Eq. (64) for $|t-t_{\min}|<v_T t_f/v_b$, which is valid for Maxwellian distribution function in Eq. (32). (For interpretation of the references to color in this figure legend, the reader is referred to the web version of this article.)

double peak structure in Fig. 6 $t_{ob}/t_p=5.9$ with single pick peak at $t_{ob}/t_p=5.3$). Such double peak with more compact foot of the pulse maybe preferable than a single peak structure with higher maximum compression achieved with larger foot, because compressed part of the beam contain more particles.

3.2. Case 2: Moderate errors ($\delta v_b/\Delta v_b\sim1\%$) in velocity modulation

If errors are reduced considerably from the 10% level to the 1% level, the compressed pulse does not change substantially. This is because the maximum of the compression ratio is determined by a small part of the pulse where the velocity errors are comparable with the thermal spread. Detailed analysis of the compression can be found in Appendix B. Here we summarize key results.

We introduced two types of errors slowly varying compared with the beam pulse. The two velocity profiles under consideration, v_{b1} and v_{b2}, have errors mostly at the beam pulse head and tail $\tau/t_p=[0,0.2];[0.8,1]$ (see Fig. 7). The first profile, v_{b1}, incorporates errors due to the smoother transition to the unperturbed initial beam velocity compared with the ideal velocity profile given by Eq. (9). In addition, the v_{b2} profile has errors according to,

$$v_{b2}-v_{b1}=-\beta v_{b0}(\tau/t_p-1/2)^3 \tag{35}$$

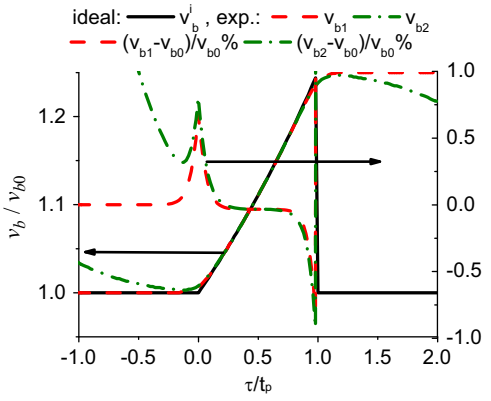

Fig. 7. The normalized beam velocity v_b/v_{b0} plotted as a function of normalized time, τ/t_p, in the tilt core. The solid (black) curve shows the ideal velocity tilt given by Eq. (9). The dashed (red) and dashed-dotted (green) curves show models of the velocity tilt and the values of the errors in percent. (For interpretation of the references to color in this figure legend, the reader is referred to the web version of this article.)

where $\beta=0.01$. We also studied scaling of compression ratio with β by increasing it ten times to $\beta=0.1$. The latter case corresponds to large, 10% errors in the velocity tilt comparable to the previous case.

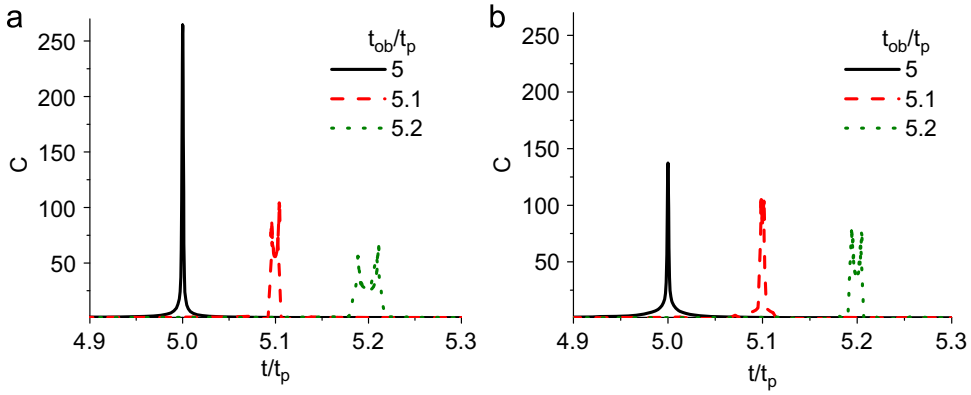

Fig. 8. (a) Plot of the compression ratio as a function of time t/t_p at three different locations $z_{ob}=z_b(t_{ob},0.5t_p)$ with $t_{ob}/t_p=5.0;5.1;5.2$ and $z=z_b(t_{ob},0.5t_p)=5.0;5.11;5.22l_p$ chosen so that the center of the pulse arrives at the target plane at a given time t_{ob} for the beam velocity profile v_{b2} shown in Fig. 7. Results are presented for a value of v_T/v_{b0} corresponding to 2×10^{-4}. For Fig. 8(b) the error in the middle of the pulse was increased 10 times to $\beta=0.1$ instead of $\beta=0.01$ in Eq. (35) for the beam velocity profile v_{b2} shown in Fig. 7.

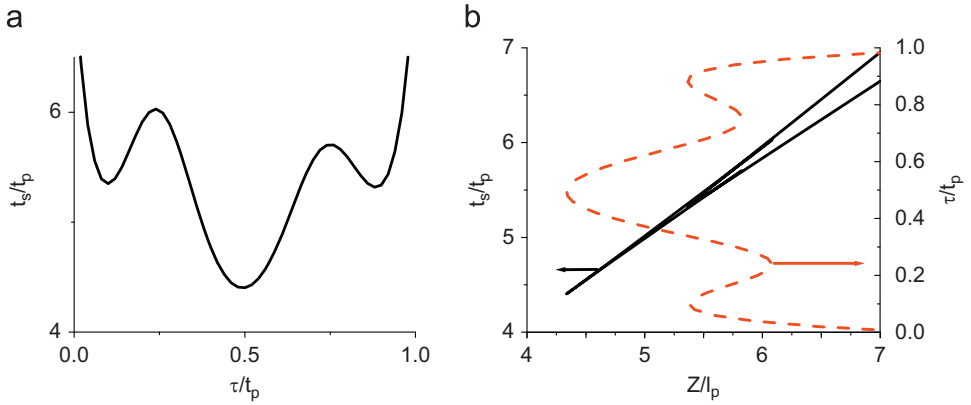

Fig. 9. The normalized time t_s/t_p when neighboring slices of the beam arrive at the same position is plotted as a function of (a) normalized time τ/t_p, and (b) beam position $z_b[t_s(\tau),\tau]/l_p$ for the beam velocity profile v_{b1}plus a ripple $v_{b1}+3\times10^{-3}v_{b0}\sin(4\pi\tau/t_p)$, where v_{b1} is shown in Fig. 7.

We introduced the cubic nonlinearity, because an error described by a linear profile results only in a change of time of the optimal compression, and does not affect the compression ratio. Furthermore, errors described by a parabolic profile do not correspond to smoother edges at the beginning and end of the pulse.

Note that large variation in the magnitude of the error does not change the maximum compression significantly [compare Fig. 8 (a and b)] where the magnitude of error was increased 10 times, from $\beta=0.01$ in Fig. 8(a) to $\beta=0.1$ in Fig. 8(b)]. The maximum compression $C_{\max}\approx v_{b0}\Delta\tau/2v_Tt$ is given by the ratio of the width of the part of the beam pulse, $v_{b0}\Delta\tau$, which compresses to within the thermal spread length, $2v_Tt$. It is shown in Appendix B [Eq. (67)] that the fraction of the pulse that compresses is given by $\Delta\tau/t_p\approx(2v_Tt_f/l_p\beta)^{1/3}$, and that

$$C_{\max}\approx\frac{1}{\beta^{1/3}}\left(\frac{l_p}{2v_Tt_f}\right)^{2/3} \tag{36}$$

From Eq. (36) it is evident that when the magnitude of the error is increased 10 times, the maximum compression decreased by only $10^{1/3}=2.2$ times, as can be seen by comparing Fig. 8(a) and (b).

3.3. Case 3: small errors ($\delta v_b/\Delta v_b\sim1\%$) but fast changes in the velocity modulation

In addition to the smooth variation in the velocity tilt, fast-changing errors during the pulse may appear in the induction bunching module. These errors can occur due to the fact that the voltage pulse is formed by several pulsed elements, and every element can introduce errors. To model these errors we added a ripple $\gamma v_{b0}\sin(\tau/\tau_\gamma)$ to $v_{b1}(\tau)$, where $\gamma=3\times10^{-3}$ and $\tau_\gamma=t_p/4\pi$ and where v_{b1} is shown in Fig. 7. Due to errors, different parts of the beam pulse compress at different times, as shown in Fig. 9. From Fig. 9 it is evident that small (less than 1%) errors in the velocity can result in a large variation in the compression time ($\sim$20%). This is because the compression time is proportional to the time derivative of the beam velocity according to Eq. (15). Moreover, due to fast changing errors during the pulse, different parts of pulse compress simultaneously at the same time or position (see Fig. 9). Correspondingly, the compressed profile may have many peaks as shown in Fig. 10. From Fig. 10 it is evident that the beam temperature only affects the height of the narrow peak at time t_s, when neighboring slices of the beam arrive at the same position, and the rest of the compressed pulse is not affected by the thermal effects.

The maximum compression $C_{\max}\approx v_{b0}\Delta\tau/2v_Tt_f$ is given by the ratio of the width of the part of the beam pulse, $v_{b0}\Delta\tau$ which compresses to within the thermal spread length, $2v_Tt$. As shown in Appendix B the fraction of the pulse that compresses is given by $\Delta\tau\approx\tau_\gamma(4v_T/\gamma v_b)^{1/2}$ and

$$C_{\max}\approx\frac{\tau_\gamma}{t_f}\left(\frac{v_b}{v_T\gamma}\right)^{1/2} \tag{37}$$

From Eq. (37) it is evident that when the magnitude of velocity error, γ, is increased by a factor of 5, the maximum compression is decreased only by a factor $5^{1/2}\simeq2.2$ as can be observed by comparing Fig. 10(a) and (b).

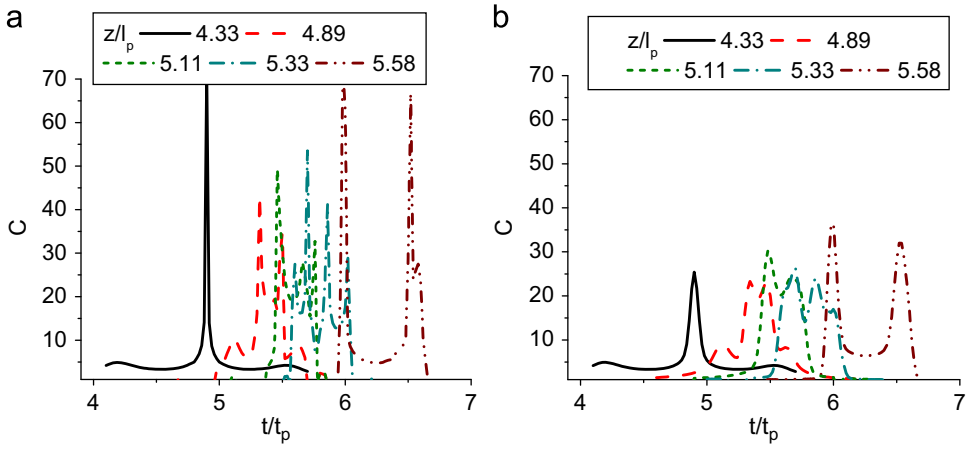

Fig. 10. Comparison of compression ratio C as a function of time at a given z for the beam velocity profile v_{b1}plus a ripple$v_{b1}+3\times10^{-3}v_{b0}\sin(4\pi\tau/t_p)$, where v_{b1} is shown in Fig. 7, for values of v_T/v_{b0} corresponding to (a) 2×10^{-4}, and (b) 10^{-3}.

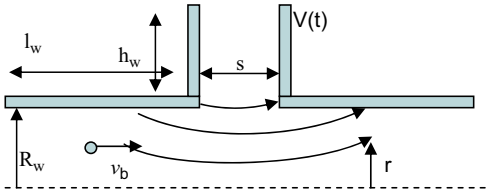

Fig. 11. Schematic of the acceleration gap of the induction bunching module. Arrows indicate the direction of the electric field; the dotted line shows the axis of symmetry.

4. Analysis of the Effects of the finite gap of the induction bunching module

For linear inductive accelerators envisioned for Heavy Ion Inertial Fusion, the induction bunching module is used for acceleration and bunch shaping. Current examples are the NDCX-I and NDCX-II experimental configuration are well described in several publications [8–10,12,22,19]. In these experiments, a potassium or lithium ion beam with energy in MeV range passes through an induction bunching module and then drifts through a neutralized drift section of several meters length. For a few centimeter gap, the beam requires 25–30 ns to cross the gap, i.e., about 10–20% of the modulating waveform duration time (about 300 ns). Therefore, transit time effects can be important. In what follows, these effects are studied analytically.

The beam velocity tilt is produced by applying an inductively-generated voltage to two electrodes, which are schematically shown in Fig. 11. The electrodes have a hole for beam passage. The hole radius is equal to the accelerator pipe radius, R_w. The presence of the hole results in an electric field profile in the gap that is intrinsically two-dimensional, spreading along the z-direction over distances of order R_w, and producing both radial electric field and longitudinal electric field components. Therefore, together with the velocity change in the z-direction, a beam ion acquires a velocity change in the r-direction. In order to calculate the radial velocity change, the radial electric field in the gap must be determined. The electric field in the gap is electrostatic, because the magnetic field is zero inside the gap, and the electric field can be obtained from Poisson's equation, with boundary condition $\varphi=0$ at the left conducting boundary, and $\varphi=V(t)$ at the right boundary (see Fig. 11). There are analytical solutions for the case of a cylindrical pipe with a gap width s, corresponding to $s\ll R_w$, $l_w\gg R_w$, and $h_w=0$. Here, l_w is the length of the washer, and h_w is the height of the washer (see Fig. 11). The solution of Poisson's equation for the on-axis potential to within 1% accuracy is given by [25]

$$\varphi(x,t)=\frac{1}{2}V(t)\left[1+\tanh\left(1.32\frac{x}{R_w}\right)\right] \tag{38}$$

Here x is the coordinate inside the bunching module. For gap widths satisfying the conditions, $s\ll3.5\ R_w$, $l_w\gg R_w$, and $h_w=0$, it is found to within 3% accuracy that the electric field on the axis ($r=0$) is given by [25]

$$E_z(x,t)=\frac{V(t)}{b\sqrt{\pi}}\exp\left[-\frac{x^2}{b^2}\right] \tag{39}$$

where

$$b=\frac{2}{\sqrt{\pi}}R_w\left[0.73+0.53(s/2R_w)^2\right] \tag{40}$$

Similarly, in the limiting case of very long washers with $l_w\to\infty$, and long vertical dimensions $h_w\to\infty$, the solution can be approximated to within 0.02% accuracy by [26]

$$E_z(x,t)=\frac{V(t)}{0.52R_w}\frac{1}{[2\cosh(1.54x/R_w)]^{1.54}} \tag{41}$$

All three solutions are compared with the numerical solution of Poisson's equation for realistic parameters of the induction bunching module and are shown in Fig. 12. As evident from Fig. 12, all solutions give nearly identical results. The change in

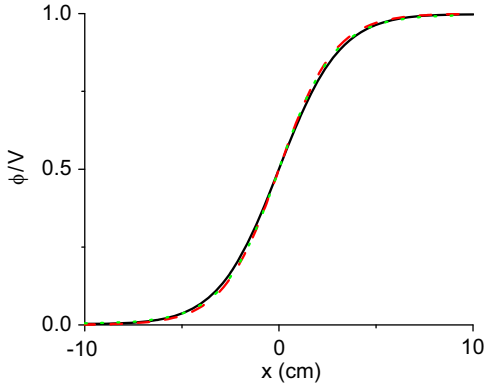

Fig. 12. Normalized electrostatic potential profile, φ/V, along the gap in the NDCX-I device with $s=2.9$ cm, $R_w=3.8$ cm, $l_w=5.08$ cm, and $h_w=5.08$ cm. The black, solid curve corresponds to the numerical solution; the red, dashed curve corresponds to Eq. (38); and the green, dotted curve corresponds to Eq. (39).

the beam kinetic energy is given by

$$\Delta E_b = e\int_{-\infty}^{\infty} E_z[x(t),t]vdt = e\int_{-\infty}^{\infty} E_z[x,t(x,\tau)]dx \tag{42}$$

Here, $t(x,\tau)$ is the time when the beam particle reaches the location x; τ denotes the time when the beam particle reaches the location of the bunching module in the approximation of infinitely small gap as before, which gives

$$t(x,\tau) = \int_0^x \frac{dx}{v(x,t)} + \int_{-\infty}^{0} dx\left[\frac{1}{v(x,t)} - \frac{1}{v_b^{in}}\right] + \tau \tag{43}$$

Recall that the initial beam velocity before interaction with the induction bunching module is v_b^{in}. Substituting for the electric field profile $E_z = V(t)f(x)$ into Eq. (42), where the function $f(x)$ describes the spatial profile of the electric field and is normalized according to $\int_{-\infty}^{\infty} f(x)dx = 1$, and calculating in a series expansion in the small parameter corresponding to the ratio of drift time through the bunching module to the pulse duration gives

$$\Delta E_b = eV(\tau) + eV'(\tau)\int_{-\infty}^{\infty}\left(\int_0^x \frac{dx}{v(x)} + \int_{-\infty}^{0} dx\left[\frac{1}{v(x)} - \frac{1}{v_b^{in}}\right]\right)f(x)dx \tag{44}$$

Here, $V'(\tau) = dV(\tau)/d\tau$ and it was assumed that the function $f(x)$ is an even function of x. Substituting into Eq. (44) for the beam velocity profile assuming a small velocity modulation in quasi-stationary potential $-V(\tau)\Phi(x)$, where $\Phi(x) = \int_{-\infty}^{x} f(x)dx$

$$v(x) = v_b^{in} + \frac{eV(\tau)}{mv_b^{in}}\Phi(x),$$

gives

$$\Delta E_b = eV(\tau)\left[1 - \frac{eV'(\tau)\gamma_w R_w}{2E_b^{in}v_b^{in}}\right] \tag{45}$$

Here, $E_b^{in} = M(v_b^{in})^2/2$ is the beam initial energy, and R_w is the wall radius and γ_w is a coefficient which is determined by the profile of the electric field in the bunching module according to one of the equivalent expressions

$$\gamma_w R_w = \int_{-\infty}^{\infty} dxf(x)\left(\int_{-\infty}^{x} dx'\Phi(x')\right) = 4\int_0^{\infty} dxf(x)x\left[\Phi(x) - \frac{1}{2}\right] = 4\int_{-\infty}^{0} dxf(x)\left(\int_x^{\infty} dx'f(x')x'\right) \tag{46}$$

For a Gaussian profile given by Eq. (39), $\gamma_w R_w = b/\sqrt{2\pi}$ and

$$\gamma_w = \frac{\sqrt{2}}{\pi}\left[0.73 + 0.53(s/2R_w)^2\right] \tag{47}$$

This gives for the gap width smaller than the pipe radius $s < R_w$, $b \approx 2\times 0.73R_w/\sqrt{\pi}$ and $\gamma_w \approx 0.33$.

The explanation of the corrections is the following: We compare the energy acquired by a beam particle in a finite size gap with that obtained in an infinitely thin gap positioned at the middle of the finite size gap. As an example, consider $V(\tau) > 0$ and $V'(\tau) > 0$, i.e., the beam particle is accelerating and the voltage grows. Because of the finite gap size, the beam particle passes through the left half of the gap more slowly than the right half of the gap; therefore it samples a smaller voltage for a longer time and the energy acquired is smaller than $V(\tau)$.

The previous calculation did not account for a small radial variation of the electric field. Away from the axis at larger radius, the electric field in the accelerator gap is spread over a shorter axial extent, see Fig. 11. Therefore, the correction to the acquired beam energy in the accelerator gap is somewhat smaller (effectively shorter R_w). The calculation is straightforward: using the Poisson law and making series for $r \ll R_w$, the electric field can be calculated near the axis according to

$$E_z(x,r) = E_z(x,r) - \frac{r^2}{4}\frac{\partial^2 E_z(x,0)}{\partial x^2} \tag{48}$$

Substituting Eq. (48) into Eq. (46) gives a radial variation of $\Delta\gamma_w R_w$ relative to the axis

$$\Delta\gamma_w R_w = -\frac{r^2}{2}\int_{-\infty}^{\infty} dxf^2(x) \tag{49}$$

Substitution of a Gaussian profile for the electric field in the gap (Eqs. (39) and (40)) first into Eq. (49) and then into Eq. (45) gives the correction to the beam energy in the radial direction,

$$\Delta E_b(r) = eV(\tau)\left[1 - \frac{eV'(\tau)\gamma_w R_w}{2E_b^{in}v_b^{in}}\left(1 - \frac{r^2}{2b^2}\right)\right] \tag{50}$$

Here, again $b \approx 2\times 0.73R_w/\sqrt{\pi} \approx 0.84R_w$ and $\gamma_w \approx 0.33$. A small variation of the beam energy as a function of radius given by Eq. (50), is of order $0.1(eV)^2 r_b^2/E_b^{in}t_p v_b R_w$ and can be very small $\sim(eV)/1000$. However, this energy spread is not removed during neutralized ballistic focus (in contrast to the space charge beam self-potential discussed in Section 2.3.2) and can give rise to thermal energy spread in induction bunching modules. For example, $\Delta E_b(r)$ is of order 100 eV for NDCX-I parameters.

For typical NDCX-I parameters the transit time, $\triangle\tau$, is $b/v_b^{in} = 30ns$, where b is given by Eq. (40). If the voltage on the induction bunching module has a high frequency ripple, the beam energy variation after passing through the bunching module, which has a finite radius, has a smoothing effect on $V(\tau)$ as the beam pulse moves through the electric field, giving $V(\tau) \to \int_{-\infty}^{\infty} \frac{V(\tau')}{\triangle\tau\sqrt{\pi}}\exp\left[-\frac{(\tau'-\tau)^2}{\triangle\tau^2}\right]d\tau'$.

5. Discussion

After passing through the induction module, the beam pulse acquires linear velocity gradient dv_b/dx and is compressed at time $t_f = (dv_b/dx)^{-1}$. Errors in the applied velocity gradient lead to imperfect compression. We have performed an analytical and numerical study of how errors in the velocity tilt acquired by the beam in the induction bunching module limit the maximum longitudinal compression, C. It is found that the compression ratio is determined by the relative errors, $\delta dv_b/dx$, in the applied velocity tilt compared with the ideal velocity tilt, dv_b/dx, and is related to the voltage errors in the induction bunching module by Eqs. (14) or (24)

$$C \sim \frac{dv_b/dx}{\delta(dv_b/dx)} \sim \frac{E_b}{t_f d(\delta U/dt)} \tag{51}$$

Here, $\delta U = Mv_b\delta v_b$, is the characteristic value of the voltage error and $E_b = Mv_b^2/2$ is the beam energy. *That is, longer compression and faster errors limit compression more.*

However, a part of the beam pulse where the errors are small, $\delta v_b \to 0$, may be compressed to much higher values which are determined by the duration of the fraction of the pulse that has such low values of velocity errors, δv_b. If we denote the $\Delta\tau$ as the pulse duration which has such low values, then the compression is

$$C \sim \frac{v_b\Delta\tau}{\delta v_b t_f} \tag{52}$$

The absolute maximum compression is given by the ratio of the width of the part of the beam pulse, $v_{b0}\Delta\tau$, which compresses to within the thermal spread length, $2v_T t_f$, that is $C_{\max} \approx v_{b0}\Delta\tau/2v_T t_f$. As described for Case 2 in Section 3 for the beam velocity error in the form $\delta v_b = -\beta v_{b0}(\tau/t_p - 1/2)^3$, the fraction of

the pulse that compresses is given by $\Delta\tau/t_p \approx (2v_T t_f/l_p\beta)^{1/3}$ and

$$C_{\max} \approx \left(\frac{v_{b0}t_p}{2v_T\beta^{1/2}t_f}\right)^{2/3}.$$

That is, the compression scales as $C_{\max} \approx \left(v_{b0}^{1/2}\Delta v_b/v_T\delta v_b^{1/2}\right)^{2/3}$ with beam velocity errors and thermal spread.

Another interesting feature of this case is that, if the target is positioned further away from the position of the compression of the central part, a double peak appears when the compressed beam suddenly arrives at this location, as shown in Figs. 6 and 8. Because at this time the tail of the pulse overtakes the head, the first peak in the double-peak structure corresponds to the tail, and the second peak to the head. The double peak structure is a well-known phenomenon in klystron theory [13,14] and was also observed in experiments with the inductive bunching module [25] and in previous simulations of longitudinal compression [9]. Note that this double-peak structure has rapid rise and low "foot" compared with the case when beam first compresses. Such double peak with more compact foot of the pulse maybe preferable than a single peak structure with higher maximum compression achieved but with a larger foot, because compressed part of the beam contain more particles.

In addition to a smooth variation in the velocity tilt, fast-changing errors during the pulse may appear in the induction bunching module. These errors can occur due to the fact that the voltage pulse is formed by several pulsed elements, and every element can introduce errors. Due to fast-changing errors, different parts of the beam pulse compress at different times, and even small errors in the velocity result in a large variation in the compression time, because it is proportional to the time derivative of the voltage. Moreover, due to fast-changing errors during the pulse, different parts of the pulse compress nearly simultaneously at the target. Correspondingly, the compressed profile may have many peaks, as described for Case 3 in Section 3. Similar to Case 2, the maximum compression is given by the ratio of the width of the part of the beam pulse, $v_{b0}\Delta\tau$, which compresses to within the thermal spread length, $2v_T t_f$, with $C_{\max} \approx v_{b0}\Delta\tau/2v_T t_f$, but the portion of the beam that compresses tightly is smaller. For example, for a model of fast errors in the form, $\delta v_b = \gamma v_{b0}\sin(\tau/\tau_\gamma)$, the fraction of the pulse that compresses is given by $\Delta\tau \approx \tau_\gamma(4v_T/\gamma v_{b0})^{1/2}$ and

$$C_{\max} \approx \frac{\tau_\gamma}{t_f}\left(\frac{v_{b0}}{v_T\gamma}\right)^{1/2}.$$

Here, τ_γ is a typical temporal scale for a change in the velocity errors, and $\gamma = \delta v_b/v_{b0} \sim \delta U/E_b$ is the magnitude of relative velocity or voltage error, as described for Case 3 in Section 3. Here, it has been assumed that velocity errors dominate the thermal spread, $\gamma = \delta v_b/v_{b0} \gg v_T/v_{b0}$. That is, the compression scales as $C_{\max} \approx (v_b/v_T\delta v_b)^{1/2}\tau_\gamma/t_f$ with beam velocity errors and thermal spread.

The effects of the finite gap width of the bunching module on compression have been studied analytically. For an ideal waveform, taking this effect into account results in a small 2% correction, which is small compared with the effects of errors, and has the effect of moving the compression plane downstream compared with the ideal case, which constitutes about 4 cm for typical NDCX-I parameters. For an experimental waveform with a fast frequency ripple, the effects of the finite gap width of the bunching module has the effect of smoothing the applied voltage over $b/v_b^{in} = 30ns$. Here

$$b = \frac{2}{\sqrt{\pi}}R_w\left[0.73 + 0.53(s/2R_w)^2\right],$$

and s is the gap width, R_w is the wall radius. Due to radial variation of the electric field profile in the gap, a beam acquires different energy as a function of radius. This variation, given by Eq. (50), is of order $0.1(eV)^2 r_b^2/E_b^{in} t_p v_b R_w$ and can be very small $\sim(eV)/1000$. However, this energy spread is not removed during neutralized ballistic focus (in contrast to the space charge beam self-potential discussed in Section 2.3.2) and can give rise to thermal energy spread in induction bunching modules. For example, $\Delta E_b(r)$ is of order 100 eV for NDCX-I and NDCX-II parameters.

Acknowledgments

Research performed under the auspices of the U.S. Department of Energy by the Princeton Plasma Physics Laboratory under Contract DE-AC02-76CH03073 and Lawrence Livermore National Laboratory under Contract DE-AC52-07NA27344. We thank the anonymous reviewers for helpful suggestions.

Appendix A. Compression of the beam pulse with relatively large errors ($\delta v_b/\Delta v_b \sim 10\%$) in velocity modulation

In this section we provide detailed analysis for the model of the velocity tilt shown in Fig. 4. The errors, in the applied velocity gradient after the beam has passed through the bunching module, are shown in Fig. A1. Because of errors in the applied velocity tilt, the gradient in the velocity is smaller than the nominal value, and the beam pulse compresses at a later time. The central part of the pulse compresses at the time when Eq. (19) gives a singularity, i.e.

$$t_{\min} = t_p + \frac{1}{|\partial v_b/\partial z|_{\max}|} \tag{53}$$

Here $\partial v_b/\partial z|_{\max} = 0.231\cdot v_b/l_p$ is the maximal value of the velocity gradient in the center of the pulse at $\tau/t_p = 0.51$ and $t_{\min} = t_p + 1/0.231 = 5.321 t_p$. From Eq. (19) it is evident that the compression ratio at time $t_{\min}$ is given by

$$C(z,t) \equiv \frac{n_b(z,t)}{n_0} = \frac{n_b(z,t_p)/n_0}{\left[\partial v_b/\partial z - \partial v_b/\partial z|_{\max}\right](t_{\min}-t_p)} \tag{54}$$

The relation between the velocity gradient and the velocity tilt as a function of time is given by Eq. (20). For the velocity profile shown in Fig. 4, the central part of the pulse has a variation in the velocity gradient below 0.4% for about one-fifth of the pulse as indicated by the two headed (green) arrows in Fig. A1. Correspondingly, this part of the pulse compresses to compression ratio above 50 according to Eq. (54), taking into account that the time

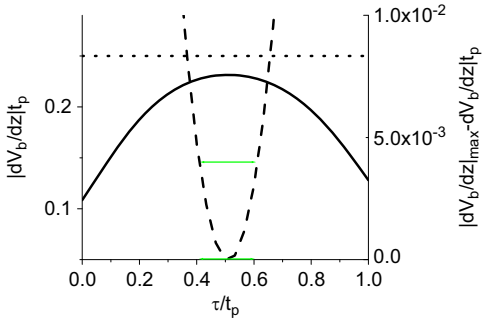

Fig. A1. The normalized beam velocity gradient $|\partial v_b/\partial z|t_p$ after the entire beam pulse passes through the bunching module is plotted as a function of normalized time, τ/t_p in the tilt core. The dotted line shows the constant for the ideal velocity tilt given by Eq. (9). The solid curve shows the velocity gradient for the model of the velocity tilt shown in Fig. 4. And the dashed curve shows the value of $|\partial v_b/\partial z|_{\max} - \partial v_b/\partial z|t_p$. The green arrow shows that portion of the beam pulse that compresses with a compression ratio above 50. (For interpretation of the references to color in this figure legend, the reader is referred to the web version of this article.)

to focus for this condition is five times longer than the beam pulse duration $t_f/t_p=5$ and $t_{min}-t_p=4.3t_p$.

The time function $t_s(\tau)$ when different parts of the ion beam pulse compress can be used instead of the velocity gradients. Both functions are related according to Eq. (20) and Eq. (15) by

$$\frac{\partial v_b(z,t)}{\partial z}=-\frac{1}{t_s(\tau)-t};\quad z=z_b(t,\tau) \tag{55}$$

The time function $t_s(\tau)$ is plotted in Fig. A2. The function $t_s(\tau)$ has a minimum in the middle of the pulse, and can be approximated near the minimum by the parabolic function

$$t_s(\tau)\approx t_{min}+\alpha(\tau-\tau_{min})^2/t_p, \tag{56}$$

where t_{min} is minimum value of $t_s(\tau)$ at $\tau=\tau_{min}$, and the α is a constant. Correspondingly, the beam pulse compression is first achieved at time, $t=t_{min}$. For the conditions in Fig. A2, the value of t_{min} is $t_{min}=5.32t_p$ rather than $t=5t_p$ for the ideal tilt. From Eqs. (16) or (17) it is evident that for the central part of the pulse with $t_s(\tau)-t_s(0.5t_p)<0.1$ and $d\Delta v_b(\tau)/d\tau\approx 0.2$, the compression ratio is above 50.

The compression ratio as a function of τ for the velocity profile in Fig. A1 is shown in Fig. A3. Maximum compression occurs at time $t_{min}=5.32t_p$, when the function $t_s(\tau)$ has a minimum, and the central part of the pulse compresses. At a slightly earlier time $t=5.3t_p$, the compression is smaller as shown in Fig. A3. If the entire pulses compresses to a point, the maximum compression is given by Eq. (30) and is equal to 564 in Case (a), and 121 in Case (b). As evident from Fig. A3, only about one-fifth of the pulse compresses for Case (a) and one-third for Case (b). Therefore, the observed maximum compression is about $120\approx(1/5)\times 564$ for Case (a), and $40\approx(1/3)\times 121$ for Case (b), i.e., one-fifth of the maximum value of compression for Case (a), and one-third for Case (b), respectively. At the position of maximum compression, when and where several slices of the beam pulse arrive at the target plane at nearly the same time, the slice position $z_b(t_{min},\tau)$ changes as cubic function of τ (see Fig. 5).

Indeed, substituting Eq. (15) into Eq. (11) gives for the derivative $\partial z_b/\partial\tau$

$$\left.\frac{\partial z}{\partial\tau}\right|_t=\frac{dv_b(\tau)}{d\tau}[t-t_s(\tau)] \tag{57}$$

Substituting the parabolic approximation for $t_s(\tau)$ given by Eq. (56), at the time of maximum compression $t=t_{min}$, gives

$$z_b(t_{min},\tau)\simeq z_b(t_{min},\tau_{min})+\frac{\alpha dv_b/d\tau}{3t_p}(\tau-\tau_{min})^3 \tag{58}$$

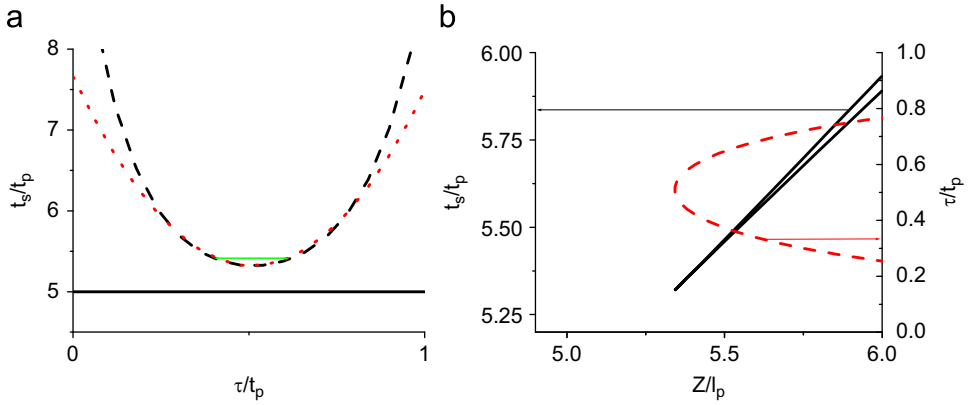

Fig. A2. (a) The normalized time t_s/t_p given by Eq. (15) when neighboring slices of the beam arrive at the same position is plotted as a function of normalized time τ/t_p in the tilt core; the solid line corresponds to the ideal velocity tilt given by Eq. (9); the dashed line corresponds to a model of the velocity tilt shown in Fig. 4; and the dotted line corresponds to the parabolic approximation in Eq. (56). The green arrow shows that portion of the beam pulse that compresses with a compression ratio above 50. (b) The normalized time $t_s(\tau)/t_p$ (black, solid) and τ/t_p (red, dashed) are plotted as functions of position $z_b[t_s(\tau),\tau]$, where different slices of the beam pulse compress. It is evident from Fig. A2(b) which slices compress at a given location and at what time. (For interpretation of the references to color in this figure legend, the reader is referred to the web version of this article.)

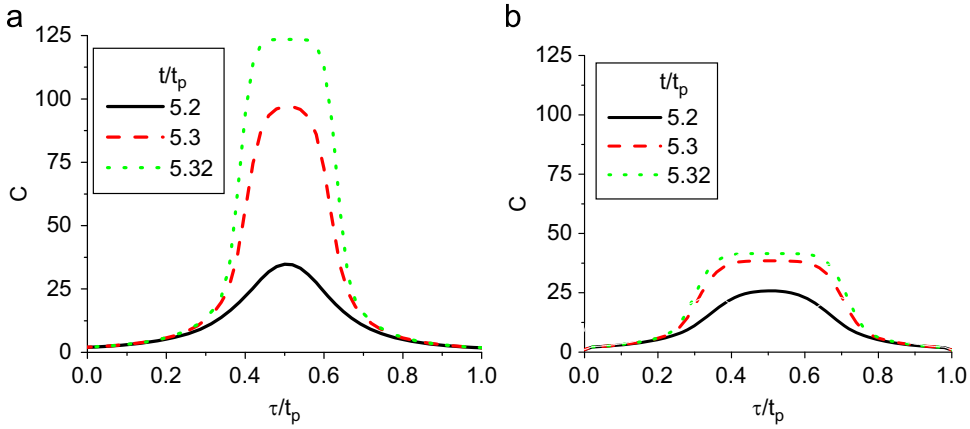

Fig. A3. Plots of compression ratio as a function of τ/t_p given by Eq. (33) at three different times $t/t_p=5.2;5.3;5.32$. At maximal compression, C is limited by thermal effects with (a) $v_T/v_{b0}=2\times10^{-4}$ and (b) $v_T/v_{b0}=10^{-3}$. If the entire pulse compresses to a point, the maximum compression $C_{max}=t_pv_{b0}/\sqrt{\pi}v_Tt_f$ would be (a) 564, and (b) 121. The observed maximum compression is 125 for case (a) because about $1/5^{th}$ of the pulse compresses, and 41 for case (b) because about $1/3^{th}$ of the pulse compresses.

Correspondingly, the fraction of the pulse that compresses within the thermal spread distance $2v_T t$ is proportional to ${v_T}^{1/3}$. For the two Cases (a) and (b) in Fig. A3, v_T differs by a factor of five, and correspondingly the fraction of the pulse that compresses also differs approximately by a factor $5^{1/3}\approx 1.7$.

In experiments, the compression ratio is measured as a function of time at a fixed position z_{ob}. The measurement time $t_m(z_{ob},\tau)$ is a function of τ according $v_b(\tau)(t_f-\tau)=z_{ob}$, or

$$t_m(z_{ob},\tau)=\frac{z_{ob}}{v_b(\tau)}+\tau \tag{59}$$

At the position near maximum compression, when and where several slices of the beam pulse arrive at the target plane at nearly the same time, $t_m(z_{ob},\tau)$ has little variation (see Fig. 1). The derivative $\partial t_m/\partial\tau|_z$ is given by

$$\frac{\partial t_m}{\partial\tau}|_z=\frac{\frac{\partial z}{\partial\tau}|_t}{\frac{\partial z}{\partial t}|_\tau}=\frac{\frac{\partial z}{\partial\tau}|_t}{v_b(\tau)}=\frac{dv_b(\tau)/d\tau}{v_b(\tau)}[t_s(\tau)-t_m] \tag{60}$$

Eq. (60) is a linear differential equation for t_m and can be solved analytically. However, an even simpler approximate solution can be obtained in the limit of a small velocity tilt, $\Delta v_b/v_b\ll 1$, when variation of t_m on the right hand side can be neglected compared with the variation of the function $t_s(\tau)$. If the target plane is positioned where a slice τ_{ob} arrives at the target $z_{ob}=z_b(t_{ob},\tau_{ob})$ at time $t=t_{ob}$, then making use of Eq. (60) with the initial condition that $t_m(z_{ob},\tau_{ob})=t_{ob}$ at τ_{ob} gives

$$t_m(\tau)\simeq t_{ob}-(t_{ob}-t_{\min})[\tau-\tau_{ob}]+\frac{\alpha dv_b/d\tau}{3v_b t_p}\left[(\tau-\tau_{\min})^3-(\tau_{ob}-\tau_{\min})^3\right] \tag{61}$$

If the target plane is located at $z_{ob}=z_b(t_{\min},\tau_{\min})$, then $t_{ob}=t_{\min}$ and $\tau_{ob}=\tau_{\min}$, which gives

$$t_m(\tau)\simeq t_{\min}+\frac{\alpha dv_b/d\tau}{3v_b t_p}(\tau-\tau_{\min})^3 \tag{62}$$

as shown in Fig. A4(a).

Substitution of the dependence of $\tau(t)$ from Eq. (62) into Eq. (16) gives the compression ratio as a function of time at the optimum focal plane at $z_{ob}=z_b(t_{\min},\tau_{\min})$ for times $|t-t_{\min}|>v_T t_f/v_b$,

$$C_f(t)=\frac{n_b(z_f,t)}{n_{b0}}=\frac{1}{(9\alpha d\Delta v_b/d\tau/t_p v_{b0})^{1/3}(t-t_{\min})^{2/3}} \tag{63}$$

The singularity of the function $C_f(t)\sim 1/(t-t_{\min})^{2/3}$ is such that a significant portion of the pulse is positioned in the (broad) wings of the pulse, $\int_{t_{\min}}^{t} n(t)dt\sim(t-t_{\min})^{1/3}$. Near the singularity point at $|t-t_{\min}|<v_T t_f/v_b$, the function $C_f(t)$ is determined by the thermal effects according to:

$$C(t)=C_{\max}\exp\left[-\frac{v_{b0}^2(t-t_{\min})^2}{(v_T t_f)^2}\right] \tag{64}$$

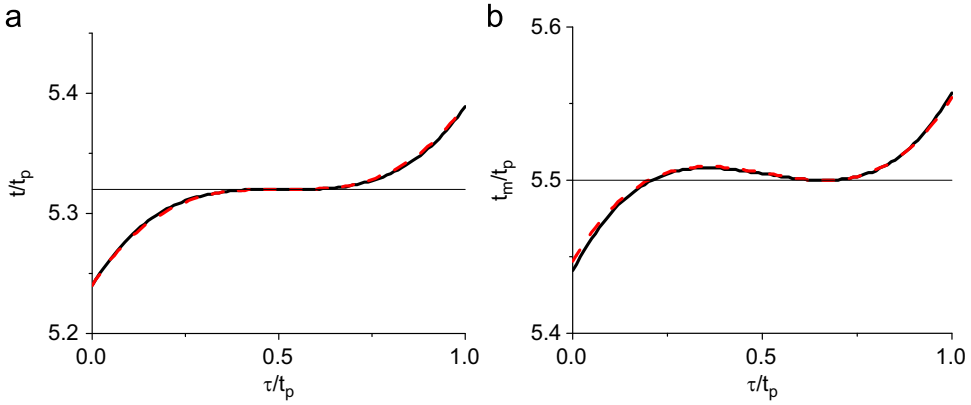

Fig. A4. Time of arrival plotted as a function of τ(solid curve) given by Eq. (59) and the approximation given by Eq. (62) (dashed, red curve) at two different positions: (a) at the point of maximum compression $z_b(t_{\min},\tau_{\min})$ and (b) at $z_b(5.5t_p,0.68t_p)$. (For interpretation of the references to color in this figure legend, the reader is referred to the web version of this article.)

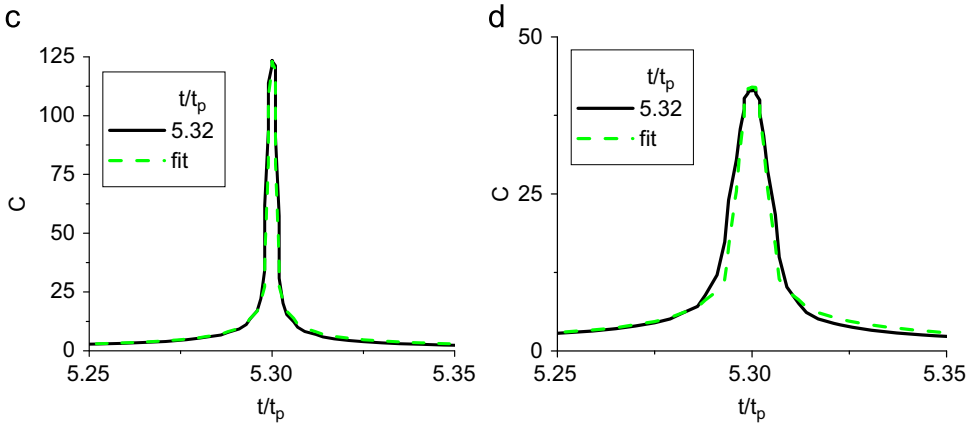

Fig. A5. Plot of the compression ratio as a function of time t/t_p at the point of maximum compression for conditions of Fig. 6. The maximum compression is limited by thermal effects with (c) $v_T/v_{b0}=2\times10^{-4}$ and (d) $v_T/v_{b0}=10^{-3}$ as in Fig. A3. Figures (c) and (d) show a zoom-in of the compression ratio as a function of time at the optimum compression location at $z_{ob}=z_b(t_{\min},\tau_{\min})=5.34l_p$ and $t_{ob}=t_{\min}=5.32t_p$ (black solid curve), and the approximation given by Eq. (63) (dashed green curve), for times $|t-t_{\min}|>v_T t_f/v_b$, and $C_f(t)$ is determined by the thermal spread and is described by a Gaussian function for $|t-t_{\min}|<v_T t_f/v_b$, which is valid for Maxwellian distribution function in Eq. (64). (For interpretation of the references to color in this figure legend, the reader is referred to the web version of this article.)

where $C_{max} \approx \Delta\tau v_{b0}/2v_T t_f$ and $\Delta\tau/t_p$ is the fraction of the pulse which compresses.

Note that for a very small thermal spread, the maximum value of compression is achieved at time $t = t_{min} = 5.32t_p$ [see Fig. A5(a)], whereas for larger thermal spread the maximum value of compression is achieved at the later time $t = 5.5t_p$ [see Fig. A5(b)], when the beam tail moves closer to the beam head over a distance of order $v_T t$, as evident in Fig. 5(c).

If the ion beam line density is measured further away from the bunching module than the optimal location corresponding to $z = z_b(t_{min}, \tau_{min})$, then the profile of the compression ratio has two peaks as a function of time. Indeed, the tail of the beam overtakes the head of the beam and two extremes appear in the phase space as evident in Fig. A4. Correspondingly, the function $t_s(\tau)$ has two roots for the solution to the equation $t_s(\tau) = t_{ob}$ [left- and right-branches of the function $t_s(\tau)$], see also Fig. A2. The arrival time $t_m(z_{ob}, \tau)$ of different slices at the target plane given by Eq. (61) is shown in Fig. A4(b). The three regions of the pulse arriving at the same time within the thermal spread contribute to the compressed part of the pulse at $t_{ob} > t_{min}$, as shown in Fig. A4(b). The double peak structure in the compression ratio is evident in Fig. A5(a) and 9(b) for times $5.5t_p$ and $5.9t_p$. For time $5.5t_p$ the double peak structure is very thin and is nearly indistinguishable on the plot. Note that in some cases this double-peak structure may be desirable because of its rapid rise and low "foot".

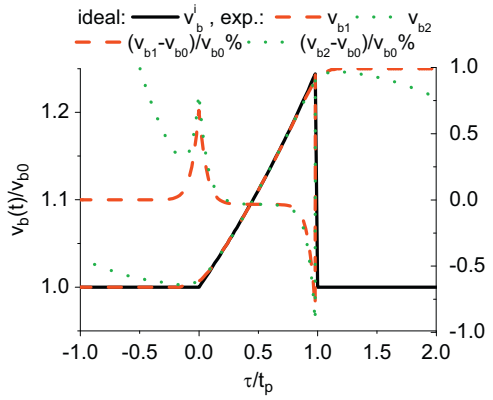

Fig. B1. The normalized beam velocity v_b/v_{b0} plotted as a function of normalized time, τ/t_p, in the tilt core. The solid curve shows the ideal velocity tilt given by Eq. (9). The dashed and dotted curves show models of the velocity tilt and the values of the errors in percents.

Appendix B. Compression of the beam pulse with Moderate errors ($\delta v_b/\Delta v_b \sim 1\%$) in velocity modulation

In the previous section, it was shown that even in the limit of large errors the compression ratio can be large because a small portion of the beam pulse compresses well where the errors are small. In this section, we study the more practical example of an even smaller error in the velocity tilt, $\delta v_b/\Delta v_b \sim 1\%$, as shown in Fig. B1. The two velocity profiles under consideration, v_{b1} and v_{b2}, have larger errors at the beam pulse head and tail $\tau/t_p = [0,0.2];[0.8,1]$ (see Fig. B1). The errors appear due to the smoother transition to the unperturbed velocity compared with the ideal velocity profile given by Eq. (9). The v_{b2} profile has additional errors

$$v_{b2} - v_{b1} = -\beta v_{b0}(\tau/t_p - 1/2)^3, \tag{65}$$

where $\beta = 0.01$. We introduced the cubic nonlinearity because an error described by a linear profile results only in a change of time of the optimal compression and does not affect the compression ratio. Furthermore, errors described by a parabolic profile do not correspond to smoother edges at the beginning and end of the pulse. The function $t_s(\tau)$ describing the compression time of different pulse slices for the velocity modulation shown in Fig. B1 is presented in Fig. B2.

Because the relative error in the function $t_s(\tau)$ is proportional to the derivative of velocity, the relative error in the function $t_s(\tau)$ is a factor of 15 larger than the relative error of the velocity modulation,

$$\frac{\delta t_s(\tau)}{t_f} \approx -\frac{t_f d\delta v_b/d\tau}{v_{b0}} = 15\beta(\tau/t_p - 1/2)^2 \sim 15\frac{\delta v_b}{v_{b0}} \tag{66}$$

Substituting $\delta t_s(\tau)$ from Eq. (66) into Eq. (57) gives

$$\delta z_b(t,\tau) \approx \delta v_b t_f = 5\beta l_p(\tau/t_p - 1/2)^3 \tag{67}$$

and substituting $\delta t_s(\tau)$ into Eq. (16) for the compression ratio at time $t = t_f$ gives

$$C_f(t) = \frac{1}{15\beta(\tau/t_p - 1/2)^2} \tag{68}$$

Therefore, even small errors in the velocity tilt lead to a noticeable change in compression time for different slices of the beam pulse. Making use of Eq. (60), the time of arrival of the beam pulse at the location of the optimum compression at $t_{ob} = t_f = 5t_p$ and $z = z_b(5t_p, 0.5t_p)$ is given by

$$t_m \approx t_{min} + 5\beta(\tau/t_p - 1/2)^3 \tag{69}$$

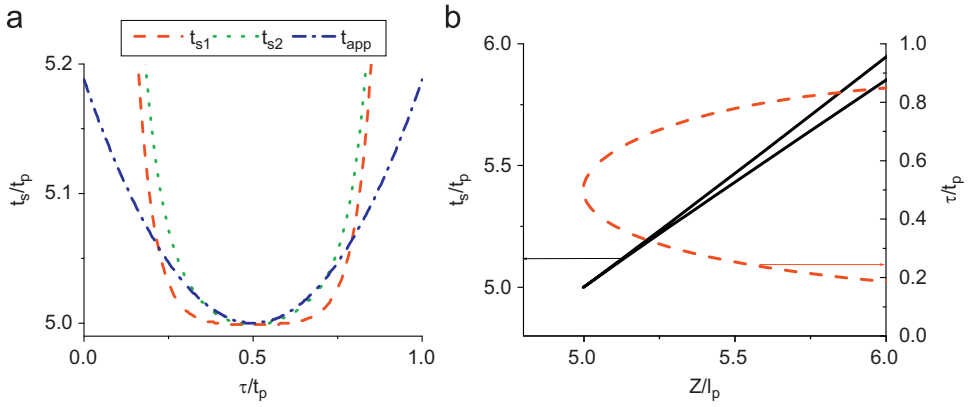

Fig. B2. The normalized time t_s/t_p when neighboring slices of the beam arrive at the same position is plotted as a function of (a) normalized time τ/t_p in the tilt core given by Eq. (15) and as a function of (b) normalized position $z_b[t_s(\tau),\tau]/l_p$, where different slices of the beam pulse compress for the two velocity tilt profiles shown in Fig. B1. The (blue) dash-dotted line corresponds to the parabolic approximation given by Eq. (66). (For interpretation of the references to color in this figure legend, the reader is referred to the web version of this article.)

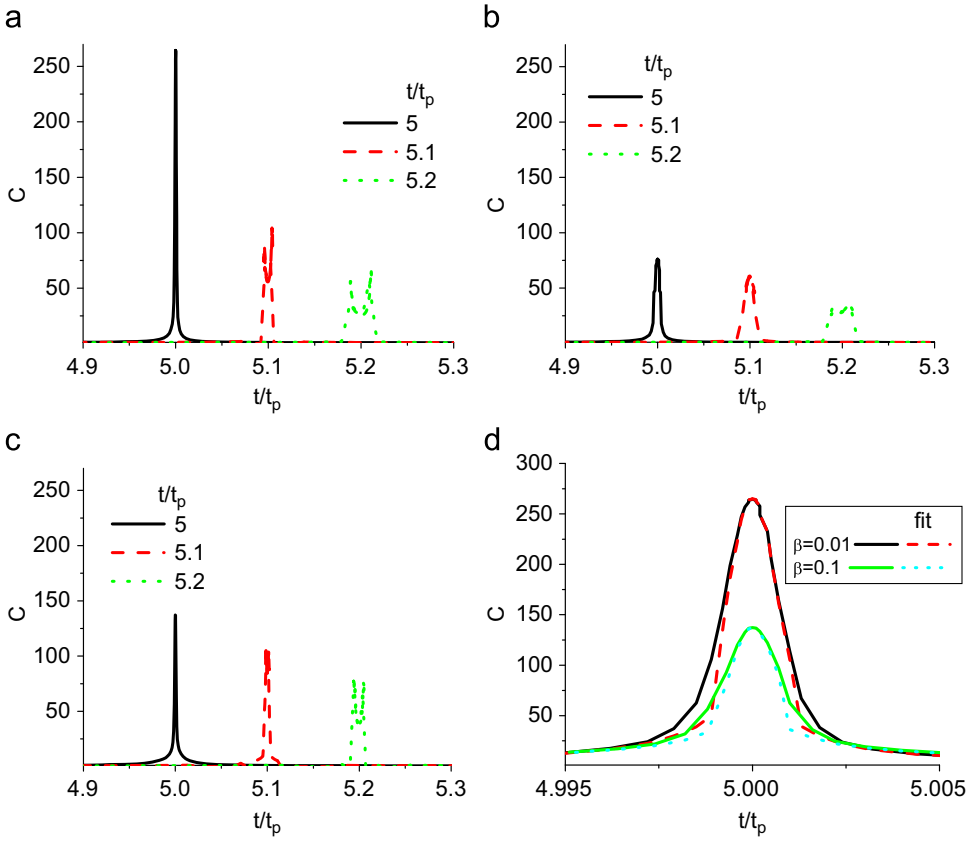

Fig. B3. Plot of the compression ratio as a function of time t/t_p at three different locations $z_{ob}=z_b(t_{ob},0.5t_p)$ with $t_{ob}/t_p=5.0;5.1;5.2$ and $z=z_b(t_{ob},0.5t_p)=5.0;5.11;5.22l_p$ chosen so that the center of the pulse arrives at the target plane at a given time t_{ob} for the beam velocity profile v_{b2} shown in Fig. B1. Results are presented for values of v_T/v_{b0} corresponding to (a) and (c) 2×10^{-4}, and (b) 10^{-3}; for Case (c) the error in the middle of the pulse was increased 10 times to $\beta=0.1$ instead of $\beta=0.01$ in Eq. (65). Figure (d) shows a zoom-in of the compression ratio as a function of time at the optimum compression location at $z_{ob}=5l_p$ and $t_{ob}=5t_p$ (black solid curve), and the approximation given by Eq. (70) (dashed red curve for $\beta=0.01$ and dotted cyan curve for $\beta=0.1$), for times $|t-t_{\min}|>v_Tt_f/v_b$, and $C_f(t)$ is determined by the thermal spread and is described by a Gaussian function for times $|t-t_{\min}|<v_Tt_f/v_b$, which is valid for the Maxwellian distribution function in Eq. (64). (For interpretation of the references to color in this figure legend, the reader is referred to the web version of this article.)

Substituting Eq. (69) into Eq. (68) for the compression ratio at the optimum focal plane gives

$$C_f(t)=\frac{1}{3(5\beta)^{1/3}[(t-t_{\min})/t_p]^{2/3}} \tag{70}$$

and is shown in Fig. B3.

Note that large variation in the magnitude of the error does not change the maximum compression significantly [compare Fig. B3(a) and (c) where the magnitude of error was increased 10 times, from $\beta=0.01$ in Fig. B3(a) to $\beta=0.1$ in Fig. B3(c)]. The maximum compression $C_{\max}\approx v_{b0}\Delta\tau/2v_Tt$ is given by the ratio of the width of the part of the beam pulse, $v_{b0}\Delta\tau$, which compresses to within the thermal spread length, $2v_Tt$. From Eq. (67) it follows that the fraction of the pulse that compresses is given by $\Delta\tau/t_p\approx(2v_Tt_f/l_p\beta)^{1/3}$ and

$$C_{\max}\approx\frac{1}{\beta^{1/3}}\left(\frac{l_p}{2v_Tt_f}\right)^{2/3} \tag{71}$$

From Eq. (71) it is evident that when the magnitude of the error is increased 10 times, the maximum compression decreased by only $10^{1/3}=2.2$ times, as can be seen by comparing Fig. B3(a) and (c) and is also shown in Fig. B3(d). The maximum compression is more sensitive to variation in the thermal velocity spread and scales according to Eq. (71) as $v_T^{2/3}$. The maximum compression in Fig. B3(a) is about 3 times larger than in Fig. B3(b), in agreement with the scaling given by Eq. (71). A factor of five smaller thermal spread in Fig. B3(a) compared with the Fig. B3(b) gives approximately a factor of $5^{2/3}\simeq2.9$ larger maximum compression ratio.

Similar to the previous section, the compression profile has a double peak structure after optimal compression. This is because both the tail and the head of the pulse compress at later times than the central part of the pulse and arrive at the target at slightly different times, with the tail arriving first. Moreover, because the compressed part of the tail arrives ahead of the main pulse, the increase in the beam line density is very fast, in contrast with the slowly increasing line density profile at the location of optimal compression [compare time $t_{ob}/t_p=5.1;5.2$ with $t_{ob}/t_p=5.0$ in Fig. B3(a) and (b)].

References

[1] P. Sing Babu, A. Goswami, V.S. Pandit, Nucl. Instr. and Meth. Phys. Res. A 642 (2011) 1;
A.V. Eliseev, I.N. Meshkov, V.A. Mikhailov, A.O. Sidorin, Physics of Particles and Nuclei Letters 7 (2010) 473;
T. Kikuchi, K. Horioka, M. Nakajima, S. Kawata, Nucl. Instr. and Meth. Phys. Res. A 577 (2007) 103;
G. Franchetti, I. Hofmann, G. Rumolo, Phys. Rev. ST Accel. Beams 3 (2000) 084201;
J.G. Wang, D.X. Wang, M. Reiser, Nucl. Instr. and Meth. Phys. Res. A 316 (1992) 112;
S. Humphries, Journal of Applied Physics 51 (1980) 2338.
[2] D.R. Welch, et al., Nucl. Instr. and Meth. Phys. Res. A 544 (2005) 236.
[3] P.K. Roy, et al., Nucl. Instr. and Meth. Phys. Res. A 606 (2009) 22.
[4] I.D. Kaganovich, R.C. Davidson, M.A. Dorf, E.A. Startsev, A.B. Sefkow, E.P. Lee, A. Friedman, Phys. Plasmas 17 (2010) 056703;

Igor D. Kaganovich, Gennady Shvets, Edward Startsev, Ronald C. Davidson, Phys. Plasmas 8 (2001) 4180.
[5] R.C. Davidson, et al., Phys. Rev. Special Topics – Accelerators and Beams 7 (2004) 104201.
[6] D.R. Welch, et al., Nucl. Instr. and Meth. in Phys. Res. A 577 (2007) 231;
D.R. Welch, et al., Phys. Rev. ST Accel. Beams 11 (2008) 064701.
[7] Scott Massidda, Igor D. Kaganovich, Edward A. Startsev, Ronald C. Davidson, Steven M. Lidia, Peter Seidl, and Alex Fridman, "Effects of errors in velocity tilt on maximum longitudinal compression during neutralized drift compression of intense beam pulses: II. Analysis of experimental data of the Neutralized Drift Compression Experiment- I (NDCX-I)", submitted to Nuclear Instruments and Methods in Physics Research A (2011).
[8] P.K. Roy, et al., Nucl. Instr. and Meth. in Phys. Res. A 577 (2007) 223;
P.K. Roy, et al., Phys. Rev. ST Accel. Beams 9 (2006) 070402.
[9] A.B. Sefkow, et al., Phys. Plasmas 16 (2009) 056701;
A.B. Sefkow, R.C. Davidson, Physical Review Special Topics on Accelerators and Beams 10 (2007) 100101;
A.B. Sefkow. Ph.D. Thesis, Princeton University (2007).
[10] P.K. Roy, et al., Phys. Rev. Lett. 95 (2005) 234801;
P. Seidel et al., Proceedings of the 2009 Particle Accelerator Conference, Vancouver, BC, Canada, TH3GAI04 〈http://trshare.triumf.ca/~pac09proc/Proceedings/papers/th3gai04.pdf〉.
[11] I.D. Kaganovich et al., Proceedings of the 2009 Particle Accelerator Conference, Vancouver, BC, Canada, TH3GAI03 〈http://trshare.triumf.ca/~pac09proc/Proceedings/papers/th3gai03.pdf〉.
[12] J.E. Coleman, et al., in: Proceedings of the Particle Accelerator Conference, Albuquerque, NM, June25–29 (IEEE catalog #07 CH37866, USA, 2007),/〈http://accelconf.web.cern.ch/accelconf/p07/PAPERS/THPAS004.PDFS〉, 2007, pp. 3516–3518;
J.E. Coleman, et al., Intense ion beams for warm dense matter physics, Ph.D. Thesis, University of California, Berkeley, 2008.
[13] J.C. Slater, Microwave Electronics, Rev. Mod. Phys. 18 (1946) 441–512;
J.C. Slater, Microwave Electronics, D. Van Nostrand Company, Inc., Princeton, 1950, p. 226.
[14] A.E. Harrison, Klystron Tubes, McGraw-Hill Book Company, Inc., New York, 1947.
[15] C.H. Kim, L. Smith, Particle Accelerators 18 (1985) 101.
[16] H. Qin, R.C. Davidson, Phys. Rev. ST Accel. Beams 5 (2002) 03441.
[17] E.A. Startsev, R.C. Davidson, New Journal of Physics 6 (2004) 141.
[18] R.C. Davidson, H. Qin, Phys. Rev. ST Accel. Beams 8 (2005) 064201.
[19] A. Friedman, J.J. Barnard, R.H. Cohen, D.P. Grote, S.M. Lund, W.M. Sharp, A. Faltens, E. Henestroza, J.-Y. Jung, J.W. Kwan, E.P. Lee, M.A. Leitner, B.G. Logan, J.-L. Vay, W.L. Waldron, R.C. Davidson, M. Dorf, E.P. Gilson, I.D. Kaganovich, Phys. Plasmas 17 (2010) 056704.
[20] M. Reiser, Theory and design of charged particle beams, second edition, WILEY-VCH, Darmstadt, 2008.
[21] J.-L. Vay, P.A. Seidl, A. Friedman, "Note on numerical study of the beam energy spread in NDCX-I", LBNL Report Number LBNL-4288E (2011).
[22] P.A. Seidl, A. Anders, F.M. Bieniosek, J.J. Barnard, J. Calanog, A.X. Chen, R.H. Cohen, J.E. Coleman, M. Dorf, E.P. Gilson, D.P. Grote, J.Y. Jung, M. Leitner, S.M. Lidia, B.G. Logan, P. Ni, P.K. Roy, K. Van den Bogert, W.L. Waldron, D.R. Welch, Nucl. Instr. and Meth. Phys. Res. A 606 (2009) 75–82.
[23] G.H. Jansen, Coulomb interactions in particle beams, Academic Press, Boston, 1990.
[24] R.C. Davidson, M.A. Dorf, I.D. Kaganovich, H. Qin, A.B. Sefkow, E.A. Startsev, D.R. Welch, D.V. Rose, S.M. Lund, Nuclear Instruments and Methods in Physics Research A 606 (2009) 11.
[25] A.B. El-Kareh, Electron beam, lenses, and optics, Academic Press, New York, 1970.
[26] E.P. Lee, Private Communication (2008).